J. Appl. Comput. Mech., 11(4) (2025) 991-1008
DOI: 10.22055/jacm.2024.47689.4765

ISSN: 2383-4536
jacm.scu.ac.ir

Shahid Chamran University of Ahvaz

Journal of Applied and Computational Mechanics

Research Paper

Dissipative Magneto-thermo-convection of Nanofluid Past through a Semi-infinite Vertical Surface with Ohmic Heating

Asra Anjum[1,2], Shaik Abdul Gaffar[2], Sateesh Kumar[1], Samdani Peerusab[3]

[1] Department of Engineering Mathematics, Koneru Lakshmaiah Education Foundation, Guntur, Andhra Pradesh, 522302, India,
Email: asraanjum84@gmail.com (A.A.); Asra.Anjum@utas.edu.om (A.A.); drsateeshdeevi@gmail.com (S.K.)

[2] Mathematics and Computing Skills Unit, Preparatory Studies Centre, University of Technology and Applied Sciences, Salalah, Sultanate of Oman,
Email: abdulsgaffar0905@gmail.com, Abdulgaffar.Shaik@utas.edu.om

[3] Department of Engineering, University of Technology and Applied Sciences Salalah, Sultanate of Oman,
Email: samdanimohd82@gmail.com, Samdani.Peerusab@utas.edu.om

Received August 07 2024; Revised December 15 2024, Accepted for publication December 20 2024.
Corresponding author: A. Anjum (asraanjum84@gmail.com)

Abstract. This study numerically investigates the non-linear, laminar convection flows of Buongiorno's nanofluid past through a semi-infinite vertical plate by considering the impacts of the magnetic parameter (*M*), heat generation and absorption (Δ), viscous dissipation (*Ec*), and ohmic heating. The research integrates the above-mentioned effects with Buongiorno's nanofluid model, addressing a significant gap in existing literature. The Buongiorno model offers a thorough framework for evaluating nanofluid dynamics since it considers both thermophoresis (*Nt*), Buoyancy ratio (*Nr*), and Brownian motion (*Nb*). A second-order flexible, implicit finite-difference Keller box method (KBM) is employed for solving the modified conservation equations mathematically, subject to physically suitable boundary conditions. Comprehensive numerical simulations are conducted to elucidate the complex interactions within the fluid. A non-similarity solution is offered that is reliant on the thermophoresis number (*Nt*), buoyancy ratio (*Nr*), Brownian motion number (*Nb*), magnetic parameter (*M*), heat generation and absorption (Δ), viscous dissipation (*Ec*), and influence of these parameters on velocity, temperature, nanoparticle concentration profiles, in the boundary layer regime is examined in detail graphically. Furthermore, an investigation is conducted into how these parameters affect the rate of surface heat transfer, the rate of mass transfer, and the rate of local skin friction. Our present code is validated using earlier studies from the literature, and an excellent correlation is achieved. The discoveries offer novelty perspectives and information about the intricate interactions between different physical phenomena in nanofluid convection, contributing to a deeper understanding of heat transmission and fluid dynamics with prospective applications in thermal management systems, and sophisticated cooling technologies. It is observed that by increasing Eckert number (*Ec*) there is a substantial hike in velocity and temperature but concentration decays, conversely, as magnetic parameter (*M*) enhances, velocity is depreciated, however, temperature and concentration profiles are elevated steadily. Also, the results obtained show that heat generation and absorption control the thermal boundary layer thickness there is a hike in velocity and temperature, but concentration depreciates significantly. Moreover, increasing the Brownian motion number enhances both velocity and temperature but there is a reduction in concentration profile, on the other hand as the buoyancy ratio (*Nr*) appreciates velocity is decelerated, however, temperature and concentration profiles have surged significantly. The results highlight how crucial it is to consider several simultaneous impacts to precisely forecast and optimize the performance of nanofluids in real-world engineering scenarios. This current study has practical implications for enhancing the design and optimization of cooling systems, electronic thermal management, and energy systems, where precise thermal control and efficient heat transfer are critical. By filling the existing research gap, this research offers valuable contributions to the field of nanofluid dynamics and thermal engineering.

Keywords: Buongiorno Nanofluid; viscous dissipation; Ohmic Heating; heat Generation and absorption; Brownian motion; Thermophoresis; Magnetic parameter.

1. Introduction

Heat transfer is crucial and significant in many industries and natural processes. Different mechanisms of heat transfer involve distinct processes and methods. Heat can be transported through three main mechanisms: conduction, convection, and radiation. Researchers introduce several techniques to improve heat transfer. These include expanding the surfaces exposed to heating or cooling sources, as in the case of heat exchangers, using fluids that are efficient heat conductors. Nanofluids are created by incorporating nanoparticles typically between 1 and 100 nanometers into a base fluid to enhance heat transfer properties. The components of the NPs are carbides, carbon nanotubes, oxides, and metals. Three of the most prevalent base fluids are water, ethylene glycol, and oil. In thermal transfer, the nanofluid finds usage in hydrogen fuel cells, heat exchangers, engine cooling, and microelectronics. Ag, Al, Cu, and other NP suspensions in normal base fluids (oil, water, etc.) can be comprehended by the nanofluid. Choi introduced the term 'nanofluid' in 1995. The base liquid's temperature properties have been significantly enhanced using uniformly suspended stable NPs in the nanofluid. Many NFs exhibit enhanced thermal characteristics, such as increased thermal conductivity at low NP concentrations. In addition, Choi identified a nonlinear correlation between NP concentration and the thermal conductivity of NFs. These results have potential applications in medicine and the advancement of nanotechnology-based cooling agents. In a nutshell, investigation into NFs is a relatively recent area of science that has great applications across many industries. Thus, this topic is crucial for both fundamental and practical study. Additionally, NFs are widely used in the Biomedical industry, defense, nuclear reactor power generation, and perhaps most importantly as cooling agents in a range of heat-transfer uses, such as electronic cooling, micropower production, solar energy, manufacturing dairy, automobiles, and heat transfer systems. Choi and Eastman's 1995 idea of nanofluid [1] has garnered some intriguing attention lately. The word "nanofluid" was originally adopted by Choi and Eastman [1] to refer to belonging to a distinct category of nanotechnology-based fluids used in heat transmission that are better at temperature than their basic fluid or regular particle fluid suspension. Regarding convective movement in NFs, Buongiorno [2] has created a two-segment link by incorporating both thermophoresis diffusion and Brownian motion development. Kanwal et al. [3] used the bvp4c technique to report the NF MHD nonlinearly radiative flows across an uneven spinning disc considering the effects of linear and nonlinear mixed convection, activation energy, and slip effects. Khan et al. [4] explored the entropy analysis of a bio-NF magnetic flow model close to a stagnation point on a contracting porous surface using the HAM technique considering viscous and ohmic heating and velocity and heat slip effects. Asia et al. [5] investigated the Carreau-Yasuda NFs 2D laminar MHD quadratic convective flow through a sheet that is stretched using the bvp4c technique. They noticed that increasing thermophoretic value, thermal conductance, and heat-generating characteristics all lead to an improvement in thermal efficiency. Elboughdiri et al. [6] theoretically analyzed a dipole-driven, two-dimensional ferromagnetic NF flow flowing across an extensible porous surface with Neild's BCs using the R-K-based shooting methodology. Many researchers are currently looking into NFs and all their varied characteristics which have led to a lot of useful studies being conducted [7- 12].

The study of magnetohydrodynamics (MHD) simulates the interaction of a magnetic field from outside with gases or liquids that conduct electricity. Many contemporary industrial operations such as ionized propulsion systems, nuclear heat transfer control, medicinal therapy, vortex control [13], and energy producers, use MHD. More Advanced working fluids with suspended NPs are being used in such systems. Thus, magneto-micropolar fluxes have a great deal to do with these kinds of systems. Boundary value problems (BVPs) related to these fluids have been studied by numerous investigators with various computational solvers in the past few years. Renu et al. [14] investigated implications of NP volume fraction, and wall thermal conductivity on mixed convection NF in a permeable vertical channel under thermal non-equilibrium conditions. Tang et al. [15] examined thermal exchange characteristics on blood bio-magnetic Darcy-Forchheimer Carreau Using homotopy analysis, other than Newtonian fluid flows in a tiny artery are investigated. To examine the 2D, MHD thermal convection flows in a sinusoidally wavy triangle filled with copper-water NF while taking heat source and sink into consideration, Islam et al. [16] investigated the Galerkin weighted residue FEM. The governing principles are given using a combination of Navier-Stokes equations, Maxwell's equations, and models tailored to nanofluidic characteristics. Magnetic fields, via the Lorentz force, can drastically modify flow properties, opening possibilities for novel technological approaches. Comparative research on thermal transport for the MHD fluid subjected to radiation past a plane and a cylindrical region was conducted [17] and concluded that the temperature domain is stronger for a cylindrical bottom. Razzaq et al. [18] investigated a non-similar solution for MHD Maxwell fluid atop an extending sheet. A generalized differential quadrature technique was developed by Ashraf et al. [19] to model the MHD peristaltic motion of blood-based NF. The mathematical modeling for MHD effects on revolving enlarging disc circulation including the transport of heat analyzed by Ahmad et al. [20]. Jan et al. [21] investigated magnetized Sisko NF, with an emphasis on the consequences of the dissipation of viscous fluid. Hussain et al. [22] investigated ramifications of electromagnetically driven NF radiative flow with a dense dissipation. Gangadhar et al. [23] studied the modified Buongiorno's NF model convective heating which causes an EMHD flow of radiative second-grade NF across a Riga Plate.

Viscous dissipation is the conversion of mechanical energy into heat because of internal friction within a fluid, which is aided by the presence of NPs. This process leads to heat generation, which is observed during production processes and can significantly influence the temperature distribution and thermal response of NF. The fluid's NP content rises. its viscosity and heat conductivity, potentially altering the extent and impact of viscous dissipation as compared to ordinary fluids. Joule heating or Ohmic dissipation can also occur in magnetized liquids in situations where thermal dissipation is caused by the magnetic field phenomena. Incorporating these into physical mathematical models is crucial for providing a more accurate assessment of transport characteristics, since they may significantly impact heat transfer mechanism. Understanding and managing viscous dissipation It is vital for enhancing system effectiveness that utilizes NFs, particularly in applications requiring efficient heat transfer and thermal management. Ignoring these impacts could result in real-world system temperatures being underestimated. Reddy et al. [24] have discussed an inclined plane's chemically viscous dissipative Buongiorno's nanofluid transport while taking thermophoresis effects and Brownian movement into account. Santhosh et al. [25] studied the mixed convection fluxes in MHD of two distinct NFs in the occurrence of viscous dissipation, joule heating, and production and absorption of heat in porous rectangular enclosure effects using the MAC finite differences methodology. Pal et al. [26] investigated the convection thermal MHD movements of micropolar liquids via an upward plate in amalgamated materials with viscous and ohmic dissipations using the RK-Fehlberg technique. Sharma et al. [27] discussed the unsteady MHD Darcy-Forchheimer viscous fluid flows across a vertically porous stretched material considering the impacts of chemical reactions, non-uniform heat source/sink, viscous and Joule heating. Li et al. [28] examined entropy analysis for viscous fluid dependent on time magnetic radiative fluxes past an infinitely permeable plate with chemical reactions in binary form, viscous, and ohmic heating using finite differences methodology. Having an emphasis on the outcomes of viscous dissipation and internal heat generation, Khan et al. [29] examined the second law analysis and mixed magnetic convection rheology of HNF flow across a surface that is stretching. The impact of joule heating and viscosity dissipation on the unstable MHD heat transfer of Jeffrey NF across extendable sheets was investigated by Shahzad et al. [30]. By employing the ND-solve approach, Hayat et al. [31] studied the entropy of mixed convective viscous flows of NF in MHD, considering the impact of heat flux, Joule heating, and chemical reaction through a stretchy cylinder.

The process of transforming electrical energy into thermal energy when an electric current passes through a resistive material is known as ohmic heating. It is also known as resistive heating or Joule heating. This effect arises because of the material's resistance to the flow of electric current, which causes electrical energy to dissipate as heat. The phenomenon that an electric current goes through when it crosses a resistance is called "Joule heat". Joule heating is significant because it may be used in an array of devices, such as hair dryers, light-emitting bulbs, clothing irons, and portable fans. Sarkar [32] looked at MHD Couette-Poiseuille flows with laminar forced convection, viscous, Joule dissipations. Shamshuddin et al. [33] investigated the impact of viscous dissipation, Joule heating, and a Cattaneo-Christov heat flux on MHD flow across a Riga plate. Mnganga [34] studied the effects of Ohmic heating, Newton heating-induced magnetic field, and convection cooling on the Couette flow of Jeffrey NF between two horizontal surfaces. Furthermore, the current literature includes a few more relevant publications [35–37].

Heat generation and absorption is a key concept in thermodynamics and heat transfer. Heat generation occurs through electrical, chemical, nuclear, mechanical, and biological processes, leading to the production of heat within a system. Examples include ohmic heating, exothermic chemical reactions, and nuclear fission. However, heat absorption includes absorbing heat from exterior sources, driven by endothermic reactions, phase changes, and various heat transfer mechanisms. These processes are critical in designing and operating thermal systems, ensuring efficient energy use and thermal management across myriad uses in engineering, environmental science, and technology. Therefore, the rate of heat generation/absorption rate should be controlled; otherwise, the resulting temperature growth/decay might fail the media. In an inclined hollow filled with a fluid-saturated permeable media, Mansour et al. [38] investigated the impact of an inclined magnetic field on unstable natural convection while considering a heat source in a solid state. Mahapatra et al. [39] examined A mixture of convection flows in an inclined hollow under the influence of magnetic effects, producing heat and heat radiation. Umadevi and Nithyadevi [40] studied magneto-convection based on water tiny fluids in a container with distinct thermal boundaries and consistent heat production. They addressed the implications of temperature generation parameters on flow, thermal fields, and heat transmission inside an enclosure. To gain a better understanding of the obstacles to commercializing NFs, Alagumalai et al. [41] created a conceptual analytical framework. Tayebi et al. [42] investigated studies of convective natural magnetic flow in an annular enclosure with NF and fins, using thermo-economic, entropy production methods. The irreversibility resulting from the main element influencing total production is no longer the thermo-effects of entropy, according to this study. Instead, the contribution of thermos-effect irreversibility to overall irreversibility is increased by magnetic forces, and enhancement of thermal transfer by using NF is discovered to be more costly when magnetic fields are prevalent. The topic of magnetohydrodynamic natural convection of NFs within a container amid thermal radiation and the effects of NP shape factor was covered by Chamkha et al. [43] in their numerical analysis employing the CVFEM method.

A semi-infinite vertical plate refers to a vertical surface extending infinitely in height and along one horizontal direction while being finite in thickness. This idealized model is used to study natural convection and BL patterns near the plate. It simplifies the analysis by eliminating edge effects, allowing focus on fluid flow and thermal properties adjacent to the plate. The semi-infinite vertical plate is crucial in examining mass, and heat transfer in buoyancy-driven flows, commonly found in atmospheric and engineering applications. Real-life applications include designing heat exchangers, cooling electronic components, and improving building ventilation systems. It is also used in environmental engineering to model pollutant dispersion in the atmosphere and oceanography for studying thermal plumes from underwater geothermal vents. Due to the numerous industrial uses for free convection flows, the momentum integral approach was initially used to study the flow of convection investigated by Pohlhausen [44] moving through a semi-infinite vertical plate. However, the solution of similarity for free convection flow was initially introduced by Ostrach [45] used a computer to mathematically solve coupled non-linear ODEs. Air was the liquid that was under examination. Gebhart and Pera [46] conducted an extensive preliminary analysis and presented the effects of transfers of mass on free convection flow across a semi-infinite vertical plate, they developed a parameter (*Nr*) and provided a comparable solution to the issue, which expresses how much of the flow's density variation is caused by chemical and heat diffusion. respectively. Subsequently, a book written by Gebhart et al. [47], refers to numerous studies that were published on this subject in varying physical settings. In each of these trials, either pure air or water was the medium that was under consideration. The density of water is influenced by both concentration and temperature since dissolved materials and suspended particles are always present, this is called the mass transfer effect. It was also believed that additional consequences, such as Soret and Dufour effects, were minimal because the concentration in air or water was thought to be less. Awati et al. [48] examined the use of NFs with varying nanoparticle types and volume fractions to significantly enhance heat transfer and alter fluid flow characteristics, with alumina, copper, and titania NPs demonstrating varying impacts past a semi-infinite static and moving flat plate [49] explored that pseudoplastic fluids on a semi-infinite plate with smaller power-law indices exhibit thinner velocity boundary layers and lower wall friction coefficients, while higher Reynolds numbers further thin the BL and reduce friction. El-Dabe et al. [50] demonstrated that magnetic fields and porous medium permeability significantly influence the velocity and heat transfer of a non-Newtonian NF near a moving vertical plate. Additionally, external cooling enhances convective heat and mass transfer, highlighting its role in controlling temperature and concentration profiles. Choudhury et al. [51] revealed that increasing radiation parameters reduces fluid temperature and skin friction for Cu-water and TiO_2-water NFs, highlighting the thermal radiation's damping effect passing through a semi-infinite plate for Cu-water and TiO_2-water NFs.

In the present work, a mathematical model is developed for steady-state laminar BL flow to explore the characteristics of BNF undergoing convection through a semi-infinite surface, incorporating effects of Magnetic parameters, viscous dissipation, Ohmic heating, and heat generation/absorption. Unlike previous studies, the literature often focused on individual effects or limited combinations of effects like MHD, viscous dissipation, Ohmic heating and heat generation/absorption effects in NF convection flows, lacking a comprehensive analysis. Traditional models also fell short in capturing the complex pattern of NFs, particularly over semi-infinite vertical surfaces. The absence of integrated studies combining BNF model with these diverse thermal and flow effects left a significant gap. Additionally, the influence of MHD on NF characteristics and heat transfer was underexplored. The article fills a critical research gap by integrating the effects taken with Buongiorno's NF theory to study non-similar convection flows providing a holistic understanding and enhanced predictive accuracy. The novelties of the present work are the simultaneous consideration of combined effects of the use of significant mechanisms such as the ohmic heating effect, magnetic field, viscous dissipation, and heat generation/absorption all contribute to this work's uniqueness in non-similar convection flows past a semi-infinite vertical plate. and PDEs which include fully two-dimensional NF flow, The study employs Buongiorno's comprehensive NF model, which includes unique effects like Brownian motion and thermophoresis, providing a more accurate representation of NF pattern in convective heat transfer scenarios. The research investigates the impact of magnetic fields on NF convection, a less commonly studied area that can significantly affect thermal management and fluid flow in various applications. The dimensionless nonlinear multi-physical BVP with related wall and free stream BCs is solved by employing the robust second-order accurate implicit finite-difference KBM. Validation using previous special instances that have been documented in the literature and authentication is also accomplished. Velocity, temperature, and nanoparticle concentration distributions are computed and visualized graphically for the influence of Brownian motion parameters (Nb), thermophoresis parameters (Nt), buoyancy ratio (Nr), Eckert number (Ec), Magnetic parameter (M), heat generation and absorption ($\triangle$). Additionally, graphs for Sherwood number (Sh), Nusselt number (Nu), and skin friction (C_f) for parameters are also shown. The simulations are relevant and provide an in-depth parametric study and investigate the impact of various factors. The article's conclusions can be applied to improve comprehension and forecasting skills in sophisticated thermal management systems, cooling system design and optimization, and precise forecasts of heat, mass transfer, and fluid flow manners by examining these intricate relationships.

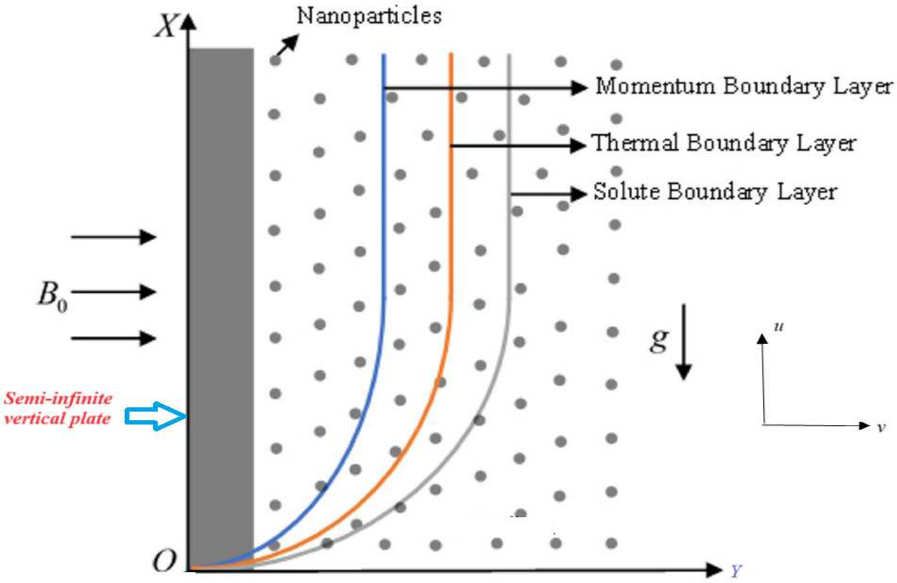

Fig. 1. Physical model and coordinate system.

2. Mathematical Model

We investigate the movement of a laminar, steady-state, incompressible convection flow NF along a semi-infinite vertical surface in an (*x*, *y*) coordinate system, considering the effects of ohmic heating, magnetic fields, viscous dissipation, heat generation/absorption. As illustrated in Fig. 1, the *x*-axis is taken along the vertical plate in an upward direction, and *y*-axis is taken normal to plate. Buoyancy effects are often caused by gradients in a dispersed species' thermal region, which drives the flow. The flow over the horizontal sheet described by Navier-Stokes becomes identical to BL equations as the characteristic value of natural convection, or the Grashof number (*Gr*), is increased indefinitely. Gravitational acceleration (*g*) exerts a downward force. The fluid is initially held at the same temperature and concentration as the semi-infinite surface. They are immediately brought to the surface temperature and concentration $T_w > T_\infty$ and $C_w > C_\infty$, respectively. The governing equations for mass, momentum, energy, and nanoparticle species (concentration) for the Buongiorno nanofluid under the boundary layer and Boussinesq approximations may be established using the model of Buongiorno [2].

The vectorial forms of the conservation equations are:

$$\nabla.\,\mathbf{V} = 0 \tag{1}$$

$$\rho_f\left(\frac{\partial \mathbf{V}}{\partial t} + \mathbf{V}.\nabla\mathbf{V}\right) = -\nabla p + \mu_f\left(\nabla^2\mathbf{V}\right) + g\left[(1-C_\infty)\rho_{f\infty}\beta(T-T_\infty) - \left(\rho_p - \rho_{f\infty}\right)(C-C_\infty)\right] + J\,\mathrm{x}\,B \tag{2}$$

$$(\rho c)_p\left(\frac{\partial T}{\partial t} + \mathbf{V}.\nabla T\right) = k_m\nabla^2 T + (\rho c)_f\left[D_B\nabla C.\nabla T + \frac{D_T}{T_\infty}(\nabla T)^2\right] \tag{3}$$

$$\frac{\partial C}{\partial t} + \frac{1}{\varepsilon}\mathbf{V}.\nabla C = D_B\nabla^2 C + \frac{D_T}{T_\infty}\nabla^2 T \tag{4}$$

Here $\mathbf{V} = (u, v)$ is the velocity vector. The Semi-infinite substrate surface (wall) and free stream (boundary layer edge) are subject to the following boundary conditions:

$$\begin{aligned} &u = v = 0,\ T = T_w, \quad C = C_w \qquad \text{at}\ \ y = 0 \\ &u \to 0, \qquad T \to T_\infty, \quad C \to C_\infty \qquad \text{at}\ \ y \to \infty \end{aligned} \tag{5}$$

The Oberbeck-Boussinesq approximation yields the linearized momentum equation, which is as follows:

$$0 = -\nabla p + \mu_f\left(\nabla^2\mathbf{V}\right) + g\left[(1-C_\infty)\rho_{f\infty}\beta(T-T_\infty) - \left(\rho_p - \rho_{f\infty}\right)(C-C_\infty)\right] + J\,\mathrm{x}\,B \tag{6}$$

The reduced BL conservation equations in an (*x*, *y*) coordinate system for the current regime are as follows:

$$\frac{\partial u}{\partial x} + \frac{\partial v}{\partial y} = 0 \tag{7}$$

$$u\frac{\partial u}{\partial x} + v\frac{\partial u}{\partial y} = \upsilon\frac{\partial^2 u}{\partial y^2} + g\left[\beta(1-C_\infty)\rho_{f\infty}(T-T_\infty) - \left(\rho_P - \rho_{f\infty}\right)(C-C_\infty)\right] - \frac{\sigma B_0^2}{\rho}u \tag{8}$$

$$u\frac{\partial T}{\partial x} + v\frac{\partial T}{\partial y} = \alpha_m\frac{\partial^2 T}{\partial y^2} + \tau\left[D_B\frac{\partial C}{\partial y}\frac{\partial T}{\partial y} + \frac{D_T}{T_\infty}\left(\frac{\partial T}{\partial y}\right)^2\right] + \frac{\nu}{\rho C_P}\left(\frac{\partial u}{\partial y}\right)^2 + \frac{\sigma B_0^2}{\rho C_P}u^2 + \frac{Q_0}{\rho C_P}(T-T_\infty) \tag{9}$$

$$\frac{1}{\varepsilon}\left(u\frac{\partial C}{\partial x}+v\frac{\partial C}{\partial y}\right)=D_m\frac{\partial^2 C}{\partial y^2}+\frac{D_T}{T_\infty}\frac{\partial^2 T}{\partial y^2} \tag{10}$$

where,

$$\alpha_m=\frac{k_m}{(\rho c)_f},\tau=\frac{(\rho c)_p}{(\rho c)_f} \tag{11}$$

The current boundary conditions are provided by:

$$\begin{aligned} &u=v=0, \quad T=T_w, \quad C=C_w, \quad \text{at} \quad y=0 \\ &u\to 0, \quad T\to T_\infty, \quad C\to C_\infty, \quad \text{at} \quad y\to\infty \end{aligned} \tag{12}$$

To transform the BVP to a dimensionless form, we introduce a stream function ψ defined by the *Cauchy-Riemann* equations, $u=\partial\psi/\partial x$ and $v=-\partial\psi/\partial y$.

The equation of continuity (1) is instantly fulfilled. The succeeding non-dimensional parameters were included to formulate the boundary conditions and governing equations in a dimensionless form:

$$\begin{aligned} &\xi=\left(\frac{x}{L}\right)^{\frac{1}{2}}, \quad \eta=C_1 y x^{\frac{-1}{4}}, \quad \psi=4\nu C_1 x^{\frac{3}{4}} f(\xi,\eta), \quad C_1=\left(\frac{Gr}{4}\right)^{\frac{1}{4}} L^{\frac{-3}{4}} \\ &Gr=\frac{g\beta(1-C_\infty)\rho_{f\infty}(T_w-T_\infty)L^3}{4\nu^2}, \; \theta(\xi,\eta)=\frac{T-T_\infty}{T_w-T_\infty}, \; \phi(\xi,\eta)=\frac{C-C_\infty}{C_w-C_\infty} \end{aligned} \tag{13}$$

Under the transformations in Eq. (13), Eqs. (8) to (10) are rendered into the following coupled nonlinear ordinary differential BL equations:

$$f'''+3ff''-2(f')^2+(\theta-Nr\phi)-M\xi f'=2\xi\left(f'\frac{\partial f'}{\partial\xi}-f''\frac{\partial f}{\partial\xi}\right) \tag{14}$$

$$\frac{\theta''}{\Pr}+3f\theta'+Nb\theta'\phi'+Nt\theta'^2+Ec\xi^2 f''^2+M.Ec.\xi^3 f'^2+\Delta\xi\theta=2\xi\left(f'\frac{\partial\theta}{\partial\xi}-\theta'\frac{\partial f}{\partial\xi}\right) \tag{15}$$

$$\frac{\phi''}{Sc}+3f\phi'+\frac{1}{Sc}\frac{Nt}{Nb}\theta''=2\xi\left(f'\frac{\partial\phi}{\partial\xi}-\phi'\frac{\partial f}{\partial\xi}\right) \tag{16}$$

where,

$$\begin{aligned} &Nr=\frac{(\rho_p-\rho_{f\infty})(C_w-C_\infty)}{\rho_{f\infty}(1-C_\infty)\beta(T-T_\infty)}, \quad Nb=\frac{\tau D_B(C_w-C_\infty)}{\nu}, \quad Nt=\frac{\tau D_T(T_w-T_\infty)}{\nu T_\infty} \\ &Gr=\frac{g\beta\rho_{f\infty}(1-C_\infty)(T_w-T_\infty)L^3}{4\nu^2}, \quad M=\frac{\sigma B_0^2 L^{1/2}}{\mu C_1^2}, \quad Ec=\frac{16\nu^2 C_1^4 L}{C_p(T_W-T_\infty)} \\ &\Delta=\frac{Q_0 L^{1/2}}{\mu C_p C_1^2}, \quad \Pr=\frac{\nu}{\alpha_m}, \quad Sc=\frac{\nu}{D_m}, C_1=\left(\frac{Gr}{4}\right)^{\frac{1}{4}} L^{\frac{-3}{4}} \end{aligned} \tag{17}$$

The transformed non-dimensional BCs become:

$$\begin{aligned} &f=0, \quad f'=0, \quad \theta=1, \quad \phi=1 \quad \text{at} \quad \eta=0, \\ &f'\to 0, \quad \theta\to 0, \quad \phi\to 0 \quad \text{as} \quad \eta\to\infty \end{aligned} \tag{18}$$

The physically interesting engineering design parameter, Skin-friction coefficient (C_f), Nusselt number (Nu) and Sherwood number (Sh) are given by:

$$\frac{1}{4\nu\mu C_1{}^3 x^{\frac{1}{4}}}C_f=f''(\xi,0) \tag{19}$$

$$\frac{-1}{k\Delta T C_1 x^{\frac{-1}{4}}}Nu=\theta'(\xi,0) \tag{20}$$

$$\begin{aligned} &\frac{-1}{D\Delta C C_1 x^{\frac{-1}{4}}}Sh=\phi'(\xi,0) \\ &\Delta T=T_w-T_\infty, \quad \Delta C=C_w-C_\infty \end{aligned} \tag{21}$$

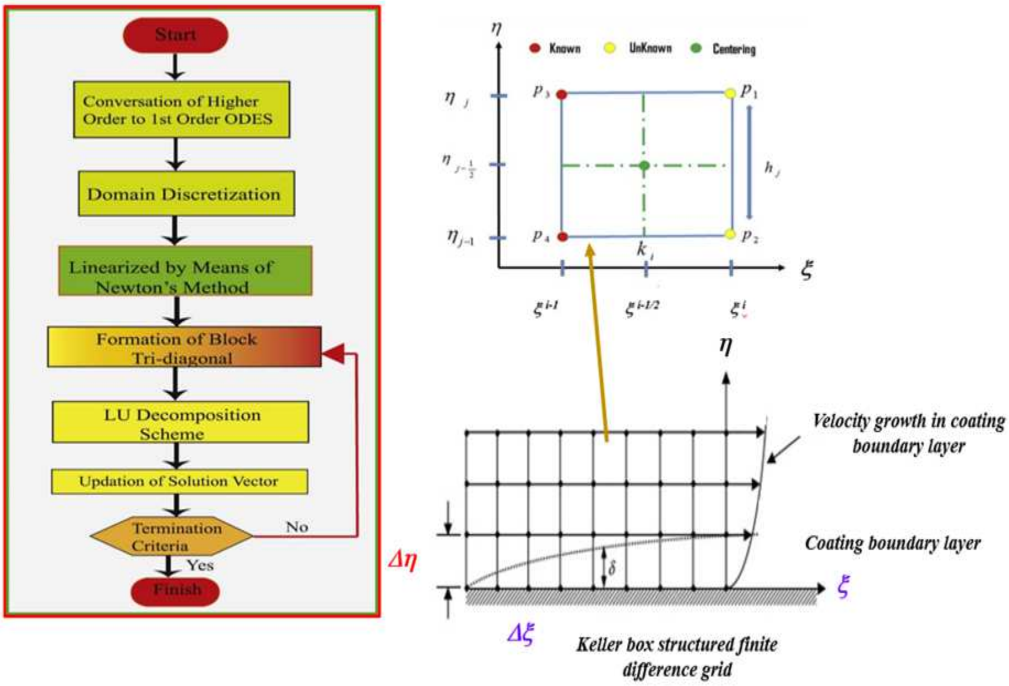

Fig. 2. Keller box procedure, box cell and boundary layer meshing.

3. Numerical Analysis Using the Keller Box Implicit (KBM) Technique

The Keller box implicit finite difference scheme [52] has been deployed to numerically solve the dimensionless ODEs (14) – (16) with BCs (18). This method remains one of the most efficient computational techniques for solving two-point BVPs. The Keller-box approach offers appealing extrapolation properties and second-order accuracy with flexible spacing. On a rectangular grid (Fig. 2), a finite-difference technique is used ("box") and converts the PDEs of the BL into nonlinear ODEs. It attains remarkable accuracy, offers steady numerical meshing characteristics, and converges quickly. By utilizing fully implicit methods with customizable stepping, the Keller box approach improves accuracy on explicit or semi-implicit schemes. Another advantage of this method is that two-coordinate (ξ,η) nonlinear partial differential equation systems can be easily accommodated, unlike other solvers such as MATLAB BVP4C, which are restricted to ordinary differential boundary value problems. In line with the physics of parabolic systems, each discretization step is fully coupled. The discrete algebra connected to the Keller-Box technique is essentially independent of any other mimicking (physics-capturing) computation methods. It attains remarkable accuracy and remains stable without any conditions. Its ability to solve partial differential equation systems including two or more spatial variables as well as a time variable is another benefit. Additional information is found in [53–57], Grid independence tests have validated the Keller-box code's accuracy in this inquiry.

The four phases involved in the Keller Box scheme are:

1. Splitting the system of N^{th} order partial differential equation down to N first order equations.
2. Finite Difference Discretization.
3. Quasi-linearization of Non-Linear Keller Algebraic Equations.
4. Block-tridiagonal elimination solution of the Linearized Keller Algebraic Equations.

3.1. Convergence analysis

Until a certain convergence threshold is met, computations are performed. The wall shear stress parameter, $\upsilon(\xi,0)$, is frequently employed as the convergence criteria in laminar boundary-layer computations [55]. It is discovered that the wall shear stress parameter is typically where BL computations exhibit the largest inaccuracy. It is worth mentioning that throughout this study, this convergence criterion is used as it is efficient, suitable, and the best yet for all the problems considered. Calculations are stopped when $|\delta\upsilon_0^{(i)}|<\varepsilon_1$, where ε_1 is a small, prescribed value.

3.2 Validation of Keller Box code

The Nusselt number (Nu) for Pr values is compared to those published in previous studies to assess the validity of the present numerical code. Table 1 exhibits this by comparing the validity of the current research to previous investigations by Chen et al. [58] for regular fluids and Narahari [59] on NFs. Based on the most recent results, a very close agreement is achieved confirming the accuracy of the present Keller box code. The data confirms that the present results validate and reinforce the findings of previous studies, indicating strong agreement and reliability in the observed trends. *Error Percentages of the comparisons are also included.*

Table 1. Comparing the local Nusselt number with the results of Chen et al. [58] for regular fluids and Narhari [59] on NFs.

Pr	Chen et al. [58]	Narhari [59]	Present Results	Error Percentage
1	0.5341	0.5344	0.5342	0.0002
7	0.8709	0.8704	0.8702	0.0002
10	0.9453	0.9447	0.9445	0.0002
15	1.0356	1.0348	1.0347	0.0001
20	1.1307	1.1027	1.1028	0.0002
50	1.3452	1.3437	1.3438	0.0001
100	1.5567	1.5547	1.5549	0.0002

4. Graphical Results and Discussions

The present section highlights the physical perspective of Buongiorno's NF flow past a past semi-infinite vertical plate incorporating effects of Magnetic parameters, viscous dissipation, Ohmic heating, and heat generation/absorption. The Keller-box finite difference technique is applied for equations (14) – (16). A detailed graphical illustration of the solution is shown in Figs. 3 to 14 utilizing MATLAB Code, on Velocity (f'), Temperature (θ) and concentration (ϕ), shear stress rate (C_f), heat transfer rate Nusselt number (Nu), mass transfer rate Sherwood number (Sh) for six dimensionless thermophysical parameters in the model, such as Brownian movement parameter (Nb), Thermophoresis parameter (Nt), Buoyancy ratio parameter (Nr), Viscous Dissipation Eckert number (Ec), magnetic parameter (M), and heat generation absorption (Δ) are presented along the radial coordinate (η). The Numerical problem comprises two independent space variables (ξ,η), default values of the following variables are $Pr = 1$, $Sc = 0.6$, $Nr = 0.1$, $Nb = 0.5$, $Nt = 0.3$, $Ec = M = \Delta = 0.5$, $\xi = 1.0$ are prescribed (unless otherwise stated).

Figures 3(a) to 3(c) shows how Eckert number ($0 \le Ec \le 4$), on (f'), (θ), (ϕ), profiles through surface regime with transverse coordinate (η). The dimensionless Eckert number $Ec = 16\nu^2 C_1^4 L / C_p(T_W - T_\infty)$ is used to measure the effect of viscous dissipation in a flow. This term $Ec\xi^2 f''^2 + M(Ec)\xi^3 f'^2$ appears in Eq. (15). Both viscous and Ohmic dissipation disappear when $Ec = 0$. High values of Ec indicate that kinetic energy is significantly converted into internal energy through viscous friction, leading to noticeable temperature changes within the fluid. Figure 3(a) illustrates that (f'), elevates when Ec rises. Higher Ec signifies greater kinetic energy relative to thermal energy, which promotes fluid motion due to viscous dissipation. Temperature (θ) rises because of this transformation of kinetic energy into thermal energy reducing viscosity, consequently increasing velocity. Figure 3(b) shows that as Ec enhances temperature also appreciates significantly, viscous dissipation causes a larger conversion of kinetic energy into thermal energy. This mechanism, combined with extra heat via Ohmic heating and internal heat generation, raises the fluid's temperature. Figure 3(c) depicts that (ϕ) declines as the Ec improves due to greater thermal energy from viscous dissipation and Ohmic heating which enhances Brownian motion of NPs. Our observations correspond with the patterns of [24, 56, 60]. Physically, the increased thermal agitation causes NPs to disperse farther away from the substrate, reducing their concentration. Additionally, elevated temperatures reduce the fluid's capacity to carry on higher NP concentrations near the BL. This elevated temperature enhances thermal diffusion, thereby reducing the concentration gradient and causing the concentration profile to decline. This underscores the inverse relationship between viscous heating and solute concentration in fluid flows. It is noteworthy that in Figs. 3(a) to 3(c) All profiles converge smoothly validating the implementation of an adequate number of infinity BCs in the free stream.

Figures 4(a) to 4(c) display the implications of the magnetic parameter ($0 \le M \le 2$), on (f'), (θ), (ϕ), profiles through the surface regime. The magnetic parameter $M = \sigma B_0^2 L^{1/2} / \mu C_1^2$ is also called the rotational Stuart number correlates the centrifugal inertial force with the Lorentzian magnetic drag force. It features in the term, $-M\xi f'$ in momentum Eq. (14) and $M(Ec)\xi^3 f'^2$ in the energy Eq. (15). Electrical non-conductivity of the NF occurs when $M = 0$ and magnetic field effects disappear. Because of the varying velocity fields, the magnetic force has a more complex effect.

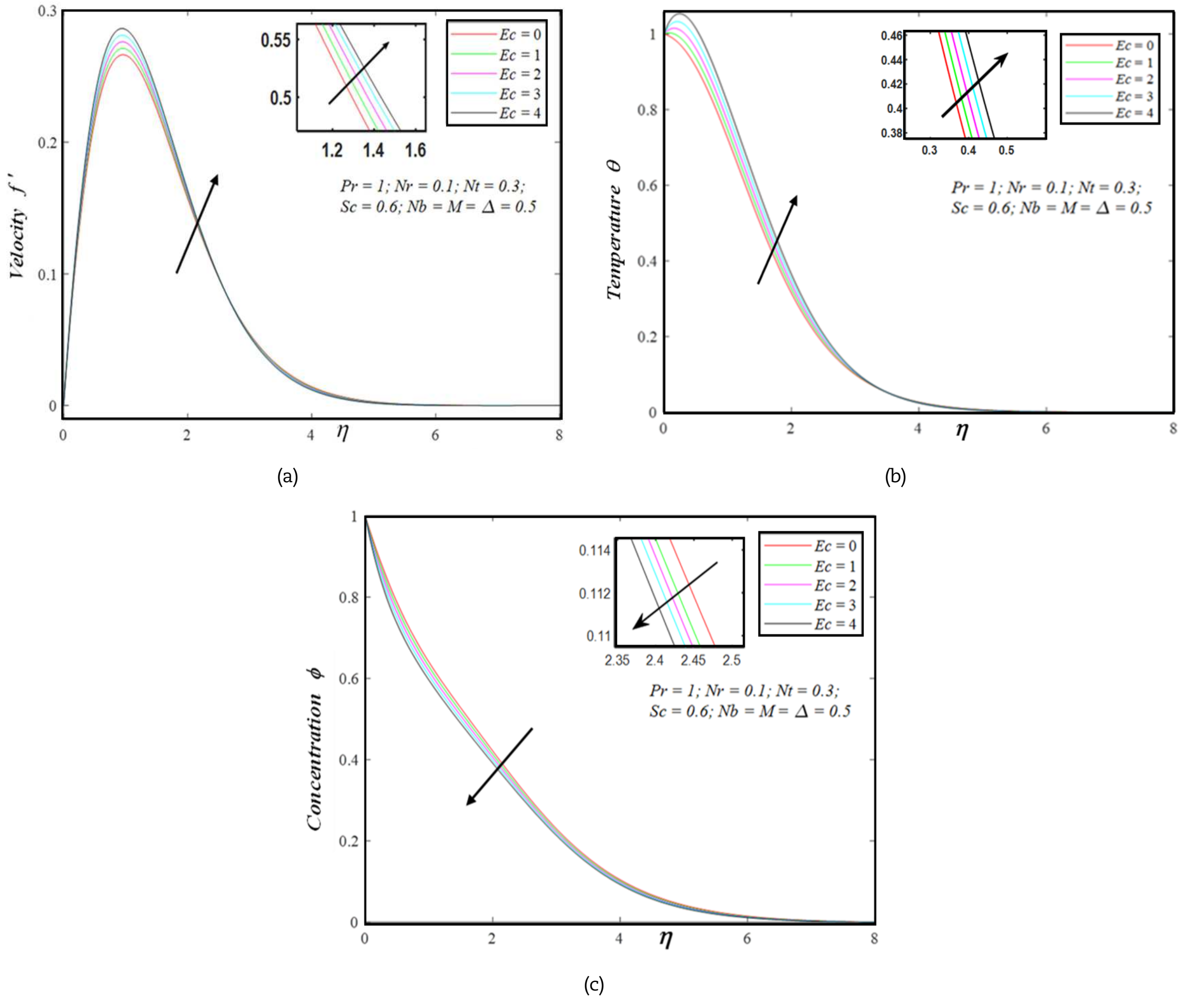

Fig. 3. Influence of Ec on (a) velocity, (b) temperature and, (c) concentration.

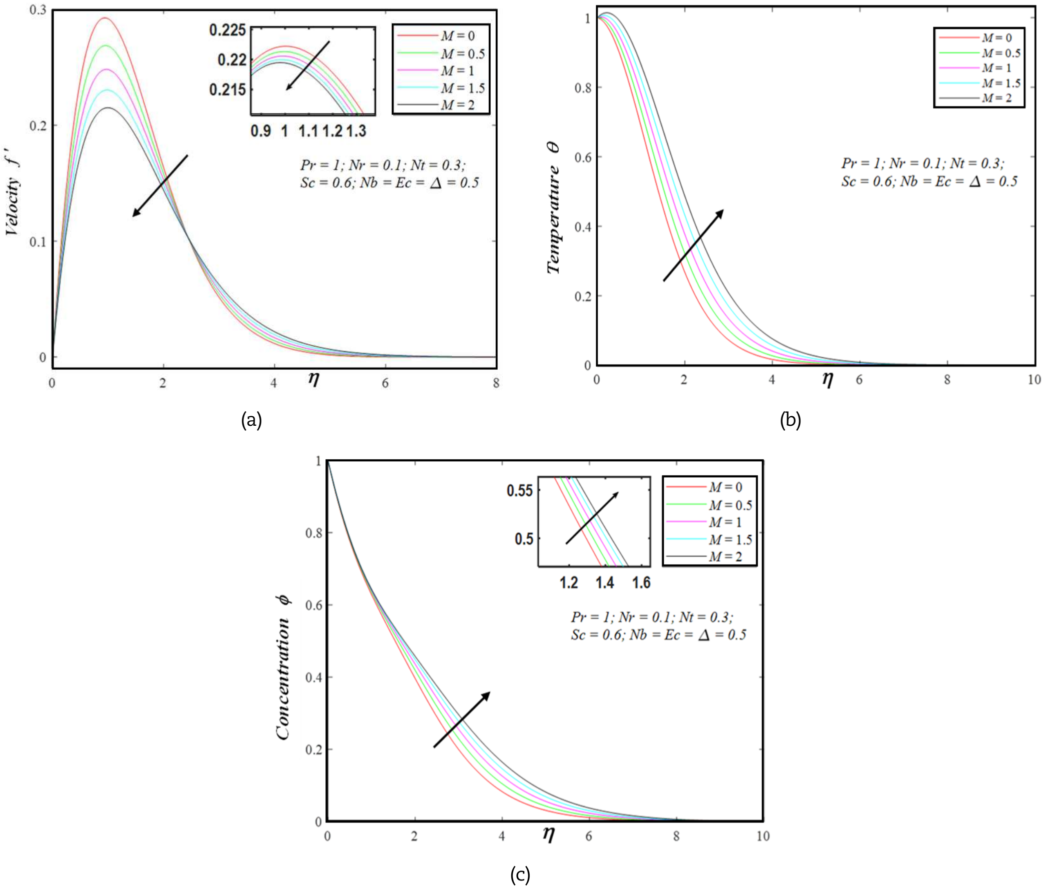

Fig. 4. Influence of M on (a) velocity, (b) temperature and, (c) concentration.

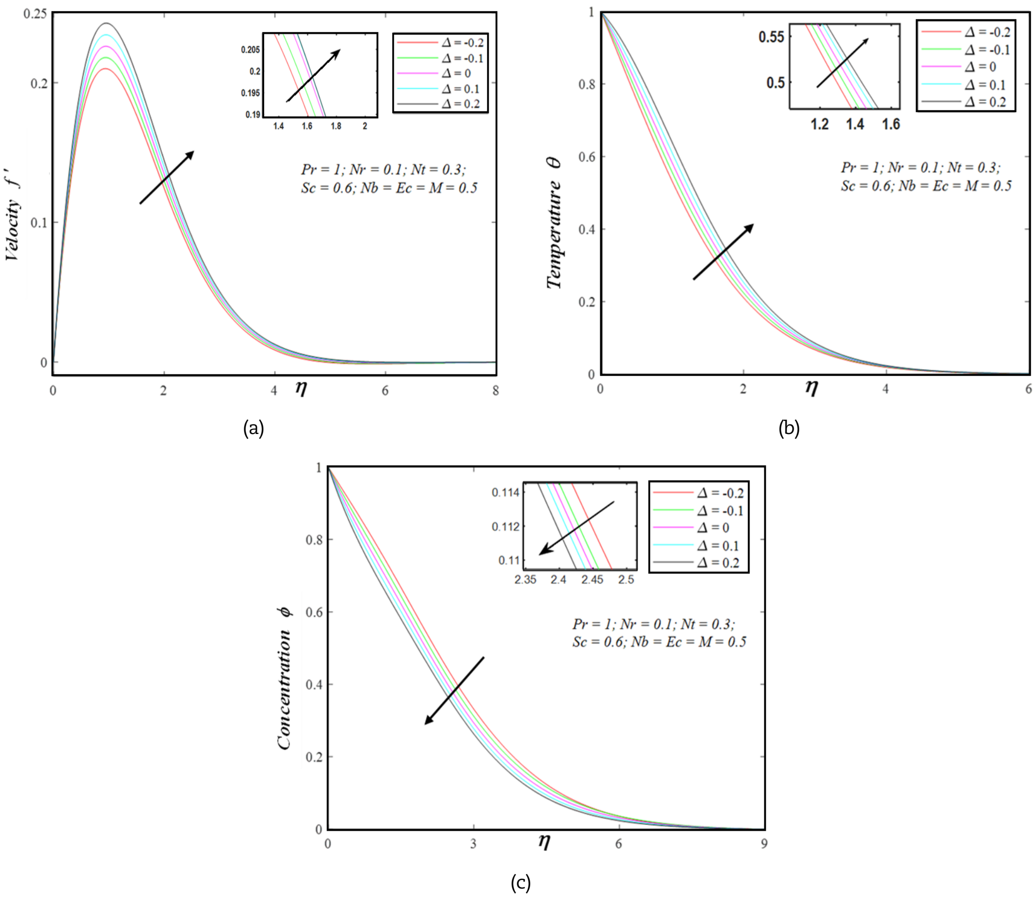

Fig. 5. Influence of Δ on (a) velocity, (b) temperature and, (c) concentration.

Figure 4(a) indicates (f') falls as M elevates because the applied magnetic field induces a Lorentz force that stops fluid motion. Magnetic drag force increases the fluid's resistance to flow, thus reducing the velocity. Additionally, this damping effect is strengthened by the magnetic field's interaction with the electrically conducting NF, which further slows down the fluid velocity. Figures 4(b) and 4(c) show how raising the magnetic parameter improves both concentration and temperature profiles by intensifying Lorentz forces, resulting in stronger fluid velocity and better mixing. The temperature rises because of the additional effort needed to drag magnetic polymer away from the action of the radial magnetic field. A boost in magnetic field strength causes the BL regime to be efficiently heated and substantially hikes the thickness of the thermal BL. Our results correspond with the patterns of [56, 60]. Physically, Lorentz's force grows with increasing magnetic parameters, slowing down fluid movement and diminishing convective transport. This reduction in convective transport allows more time for mass diffusion to occur, enhancing the concentration profile. Thus, stronger magnetic fields lead to greater mass accumulation due to decreased fluid movement. It is noteworthy that in Figs. 4(a) to 4(c) The fact that every profile in the free stream converges smoothly suggests that the right significant infinity BCs have been adopted.

Figures 5(a) to 5(c) emphasize the influence of heat generation/absorption ($-0.2 \le \Delta \le 0.2$), on (f'), (θ), (ϕ), profiles are illustrated. The heat generation and absorption term $\Delta = Q_0 L^{1/2} / \mu C_p C_1^2$, this term $+\Delta\xi\theta$ appears in the heat equation (15). Figures 5(a) and 5(b) demonstrates that increasing causes more energy to be deposited in the fluid, leading to higher temperatures. This rise in temperature boosts fluid expansion and buoyant forces, resulting in higher fluid velocity profiles. As a result, the increased velocity promotes quicker convective heat transfer, results prominent temperature gradient, and improves thermal transport properties in the system. Furthermore, from Fig. 5(c) we observe that higher values intensify temperature gradients, leading to better thermal convection and fluid motion. This enhanced fluid mobility leads to more efficient mixing, which reduces solute BLT near the surface and results, in concentration profile depreciation as the improved convection disperses the solute more effectively, resulting in a thinner concentration BL and overall lower concentration gradients throughout the system. Physically, increasing the heat generation and absorption parameter raises the thermal energy within the fluid, enhancing molecular agitation which boosts velocity and temperature profiles. However, this increased thermal energy also accelerates NP diffusion, leading to a more rapid dispersion of particles and thus a decline in concentration profile near the surface. It is noteworthy that in Figs. 5(a) to 5(c) The smooth convergence of all profiles in the free stream has infinite BCs that are appropriately massive.

Figures 6(a) to 6(c) Shows the impact of Brownian motion ($0.4 \le Nb \le 1.2$), on (f'), (θ), (ϕ), profiles through surface regime with transverse coordinate (η). (Nb) is defined as ratio of the Brownian diffusion coefficient to thermal diffusivity of base fluid. This parameter is utilized to quantify effects of (Nb) on heat, mass transmission characteristics of NFs. Mathematically, it can be expressed as: $Nb = \tau D_B (C_w - C_\infty)/\nu$. The term $+Nb\theta'\phi'$ appears in the thermal equation (15) and $+Nt/NbSc\theta''$ appears in the concentration equation (16). According to the Buongiorno formulation [2], higher values of Nb indicate smaller NPs, and varying this parameter produces a change in ballistic collisions. In Fig. 6(a) Velocity (f') is enhanced although a stronger elevation is computed in the former with greater Nb values. Brownian motion also modifies the NF thermal conductivity and the propensity for heat transmission in the NF. As a result, the increased random motion of the NPs modifies the thermal performance as well, and the momentum field experiences this influence through thermal buoyancy. As Nb increases, the temperature (θ) is positively affected across the BL regime, as seen in Fig. 6(b). There is also a significant change in the topology of the temperature profiles further from the substrate (wall) at very high Nb values. Raising the temperature aggravates the motion of the NPs and ballistic collisions. Consequently, chaotic Brownian motion is increased even further.

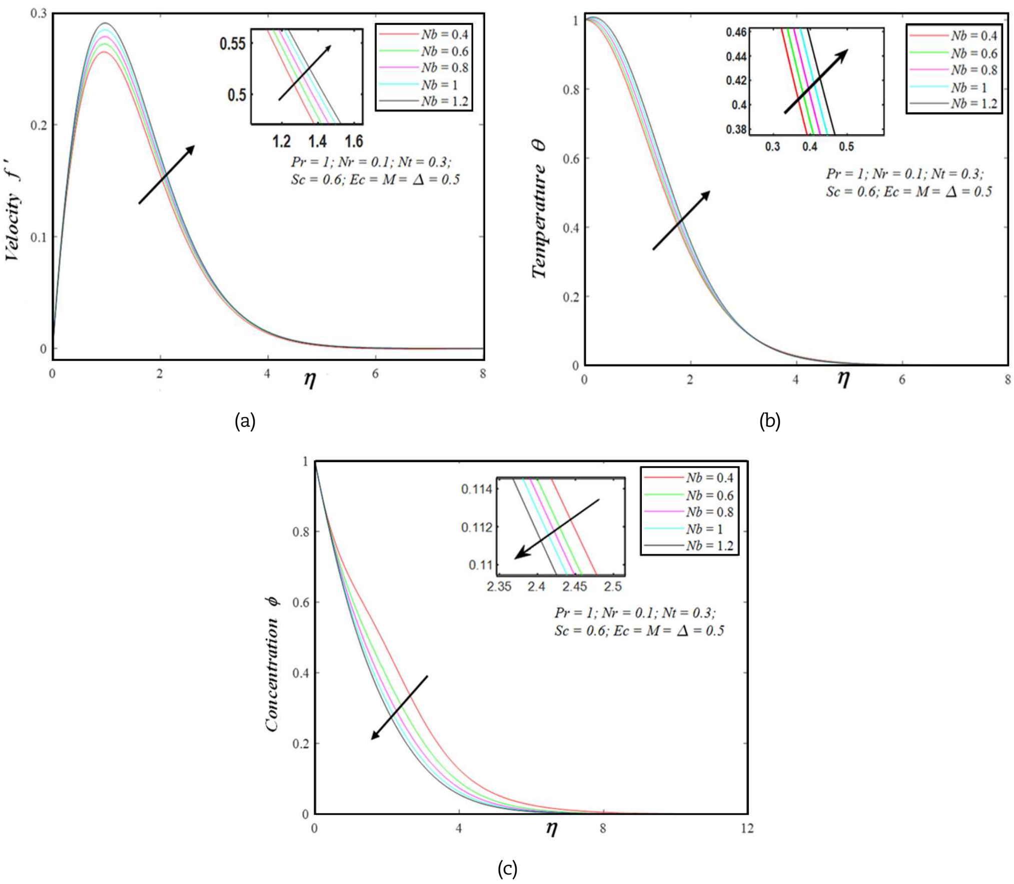

Fig. 6. Influence of Nb on (a) velocity, (b) temperature and, (c) concentration.

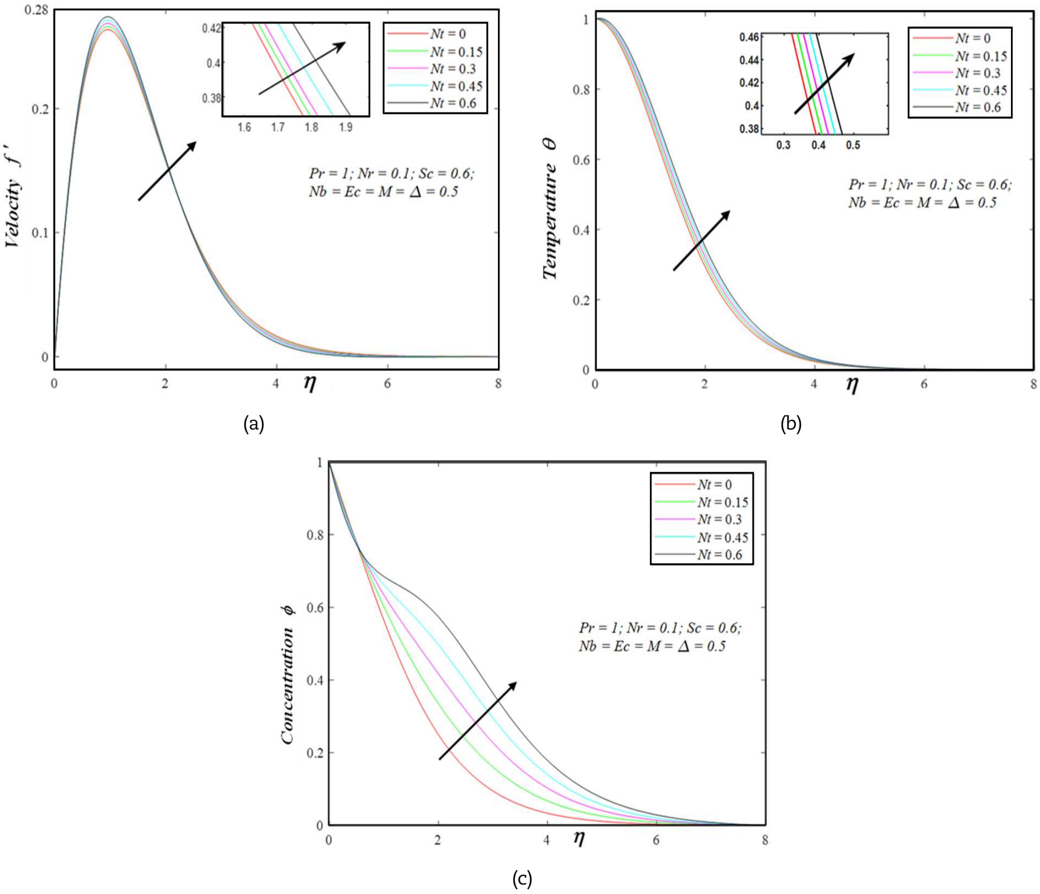

Fig. 7. Influence of Nt on (a) velocity, (b) temperature and, (c) concentration.

The increased heat conduction in the regime and the improved micro-convection surrounding the NPs are also influenced by the change in thermal conductivity with greater Brownian motion. As a result, the thermal BL gets thicker due to the heating effect. Although the fluid's molecules and NPs are always moving, there is a noticeable shift in temperature overall. Brownian motion, however, predominates in the random thermal motion of the NPs. It observed in Fig. 6(c) that as Nb is increased, however, the intensification in ballistic collisions curtails the dispersion of NPs, leading to a discernible drop in the concentration of NFs values, Hence, concentration BLT is reduced which is important in fine-tuning coating structure during the manufacturing process. Our results concur with the trends of [24, 56, 60, 61] who have also shown that the greater viscosity acts to accelerate the flow and heat convection but depress mass transfer rates. The physical significance of these observations lies in the complex interplay between Brownian motion and NF dynamics. As Nb increases, nanoparticles experience enhanced random movement, facilitating more efficient thermal diffusion and increasing fluid velocity. This phenomenon is crucial in settings where efficient heat transport is necessary, like cooling structures and thermal management in engineering. However, the reduction in concentration gradient signifies a more homogeneous dispersion of NPs, which can affect processes reliant on localized concentrations, such as drug delivery or materials synthesis. The fluid's Brownian motion is significantly impacted by increasing Nb levels because of the nanoparticles' random mobility. It is noteworthy that in Figs. 6(a) to 6(c) All profiles converge smoothly validating the implementation of an infinite number of BCs in the free stream that is suitably huge.

Figures 7(a) to 7(c) Depicts influence of the thermophoresis parameter ($0 \le Nt \le 0.6$) on (f'), (θ), (ϕ), profiles on surface regime with transverse coordinate (η). Driving NPs under a temperature gradient is known as thermophoresis, Nt quantifies impact of thermophoretic force, which drives nanoparticles from hot regions to cold regions causing the fluid temperature to be modified within a fluid. The definition of thermophoresis parameter is ratio of thermophoretic diffusion coefficient to thermal diffusivity of base fluid. Mathematically, it can be expressed as: $Nt = \tau D_T(T_w - T_\infty)/\nu T_\infty$. This term $+Nt\theta'^2$ appears in the thermal equation (15) and $+Nt/NbSc\theta''$ appears in the concentration equation (16). According to the Buongiorno formulation [3], thermophoretic body force has a direct impact on NP diffusion. From Fig. 7(a), an increase in Nt accelerates velocity (f') profile. The increasing thermophoresis parameter value enhances temperature (θ) in Fig. 7(b) and considerably boosts the concentration (ϕ) in Fig. 7(c) These trends are sustained at all distances transverse to the inclined substrate. However, while asymptotic decays occur from the wall to the free stream for all temperature profiles, the nanoparticle concentration profile is only a decay for $Nt = 0$, which has not been identified previously in the literature. As Nt increases, the topology is flipped from a convex to a concave one for $Nt = 0.6$. With subsequent elevation in the thermophoresis parameter, a peak in nanoparticle concentration emerges progressively further from the wall. Eventually, for $Nt > 0.15$ the curves descend smoothly to the free stream. Overall, stronger thermophoresis elevates the thermal and concentration BLT, which inevitably influences the structure of the coating regime. The impact of a higher thermophoretic temperature gradient is significant on all transport characteristics, confirming the important role it plays in NF mechanics. Our findings support the patterns of [24, 56, 60, 61]. Physically, this signifies that a stronger thermophoretic force leads to enhanced momentum, heat, and mass transfer, reflecting more pronounced thermal and solute gradients in the NF flow. The two most intriguing aspects of the BNFs model are thermophoresis and Brownian motion characteristics. In essence, these characteristics raise the fluid's temperature which is essential for improving mass transport and thermal procedures for a variety of purposes. It is noteworthy that in Figs. 7(a) to 7(c) All profiles converge smoothly in the free stream, confirming that an adequately large infinity boundary condition has been deployed.

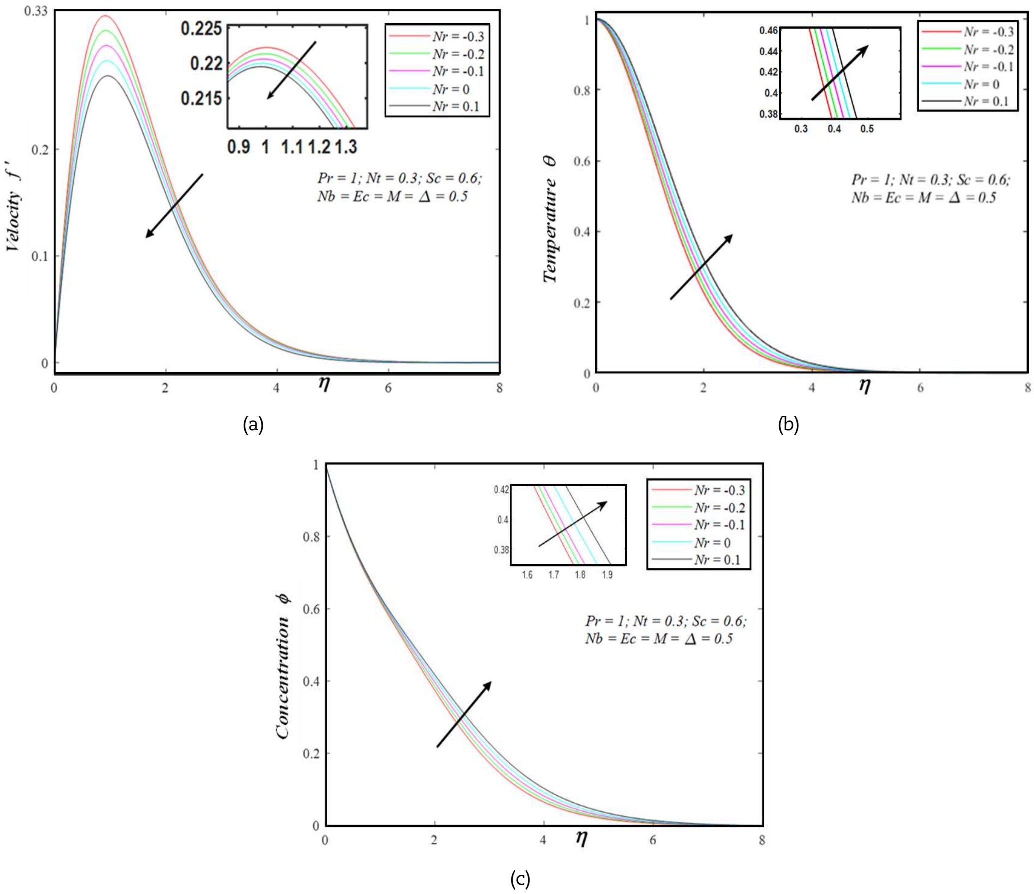

Fig. 8. Influence of *Nr* on (a) velocity, (b) temperature and, (c) concentration.

Figures 8(a) to 8(c) elucidate the impact of the combined Buoyancy ratio parameter (-0.3 ≤ *Nr* ≤ 0.1) on profiles (f'), (θ), (ϕ), through surface regime with transverse coordinate (η). Dual natural convection currents mobilized by temperature and NP species are present. The combined buoyancy effect is simulated via the term, $+(\theta - Nr\phi)$ in the momentum Eq. (14) in which $Nr = (\rho_p - \rho_{f\infty})(C_w - C_\infty)/[\rho_{f\infty}(1 - C_\infty)\beta(T - T_\infty)]$, (*Nr*) quantifies the relative influence of thermal, and concentration buoyancy forces on fluid flow. It's defined as the ratio of concentration buoyancy force to thermal buoyancy force. The regime exhibits buoyancy from both thermal and nanoscale species, resulting in dual natural thermo-solute convection. If *Nr* < 0, forces of thermal buoyancy and species buoyancy forces are opposed to each other. If *Nr* = 0, forced convection occurs, and buoyancy forces disappear. For *Nr* > 0, the buoyancy force helps the other. As seen in Fig. 8(a) Velocity (f') is suppressed with positive *Nr* but is enhanced with negative *Nr*. In other words, assistive buoyancy damps the primary flow whereas opposing buoyancy This reduction weakens the buoyancy-driven movement, tending to a decrease in fluid velocity. Consequently, with less buoyancy force driving fluid motion, the convective heat transfer process is hindered, resulting in the depreciation of velocity profiles in the system. Figures 8(a) and 8(b) demonstrates that an increment of *Nr* strengthens the buoyancy-driven flows. This augmentation enhances fluid motion, facilitating more effective mixing and transport of heat and solute. Consequently, (θ) and (ϕ) profiles are appreciated. Notably, both temperature and concentration profiles show an upward trend, signifying the heightened internal buoyancy forces improve heat and mass transfer. This results in higher thermal, solute gradients near the surface, causing increased (θ), (ϕ) levels within the boundary. Our outcomes align with the observed trends of [24, 56, 61, 62]. Physically, this signifies that stronger buoyancy effects lead to more efficient energy and species transport in the fluid this is essential for precisely estimating flow response and maximizing mass and heat transfer in a variety of technical applications. f' converges to a value close to 1 for all values of *Nr*. The convergence to this asymptotic value implies that beyond a certain point, further increases in η have minimal effects on (f'). This suggests that the system reaches a steady state or equilibrium condition. All the curves eventually converge as η increases, showing that at a sufficient distance, the temperature becomes negligible regardless of *Nr* values. (θ) increases monotonically and approaches 0 as η reaches around 6. (ϕ) increases monotonically and approaches 0 as η reaches 6 to 8.

Figures 9(a) to 9(c) demonstrate the impacts of Eckert number (*Ec*) on (C_f), (*Sh*), (*Nu*) along the surface regime. Figure 9(a) As *Ec* increases, indicating higher viscous dissipation, more kinetic energy is converted to thermal energy, which enhances the fluid's velocity gradients, thereby increasing (C_f). Figure 9(b) The increased temperature gradients also intensify mass transfer, raising the (*Sh*). However, in Fig. 9(c) the added thermal energy reduces the temperature difference between fluids, surface decreasing *Nu*, which measures heat transfer efficiency. Physically, this conversion increases the fluid's velocity gradients near the surface, thereby raising skin friction. The higher thermal energy also enhances NP diffusion, leading to more effective mass transfer and thus increasing *Sh*. However, the elevated internal thermal energy reduces the temperature gradient between fluid, and surface which is the driving force for convective heat transport, resulting in a lesser *Nu* value. Thus, while momentum mass transfer is enhanced, the efficiency of heat transmission diminishes due to the reduced temperature differential. In electronic cooling systems, such as those in high-performance computers, increased viscous dissipation from rapidly moving coolant fluids generates heat, enhancing fluid velocity and mass transfer rates, analogous to higher C_f, *Sh*. However, the reduced temperature gradient between the coolant and the heated components leads to less efficient heat removal, reflecting a lower Nusselt number.

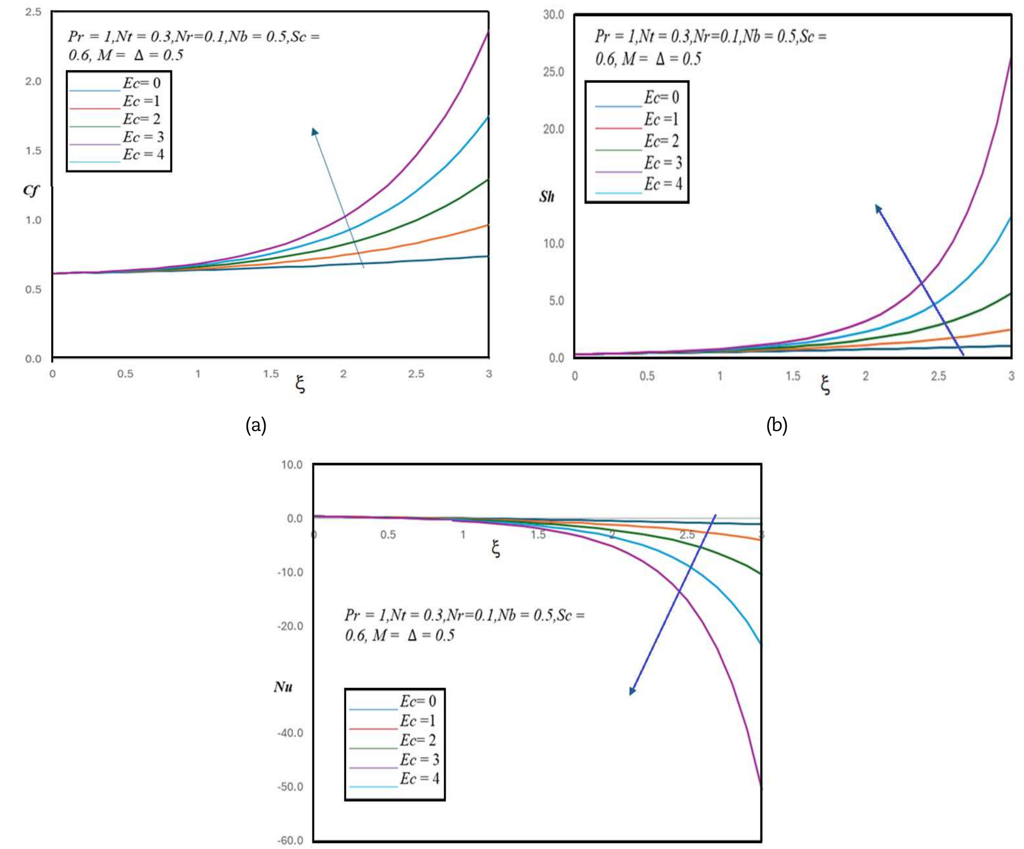

(a) (b)

(c)

Fig. 9. Influence of *Ec* on (a) skin friction, (b) Sherwood number and, (c) Nusselt number.

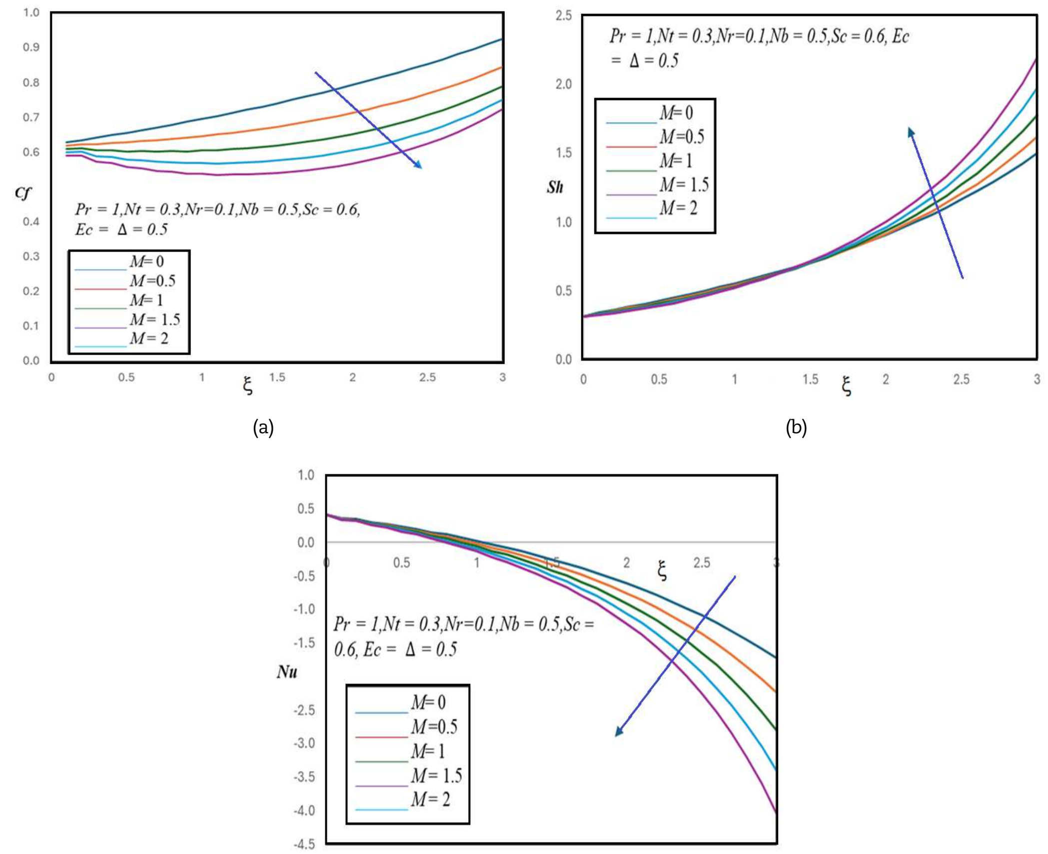

(a) (b)

(c)

Fig. 10. Influence of *M* on (a) skin friction, (b) Sherwood number and, (c) Nusselt number.

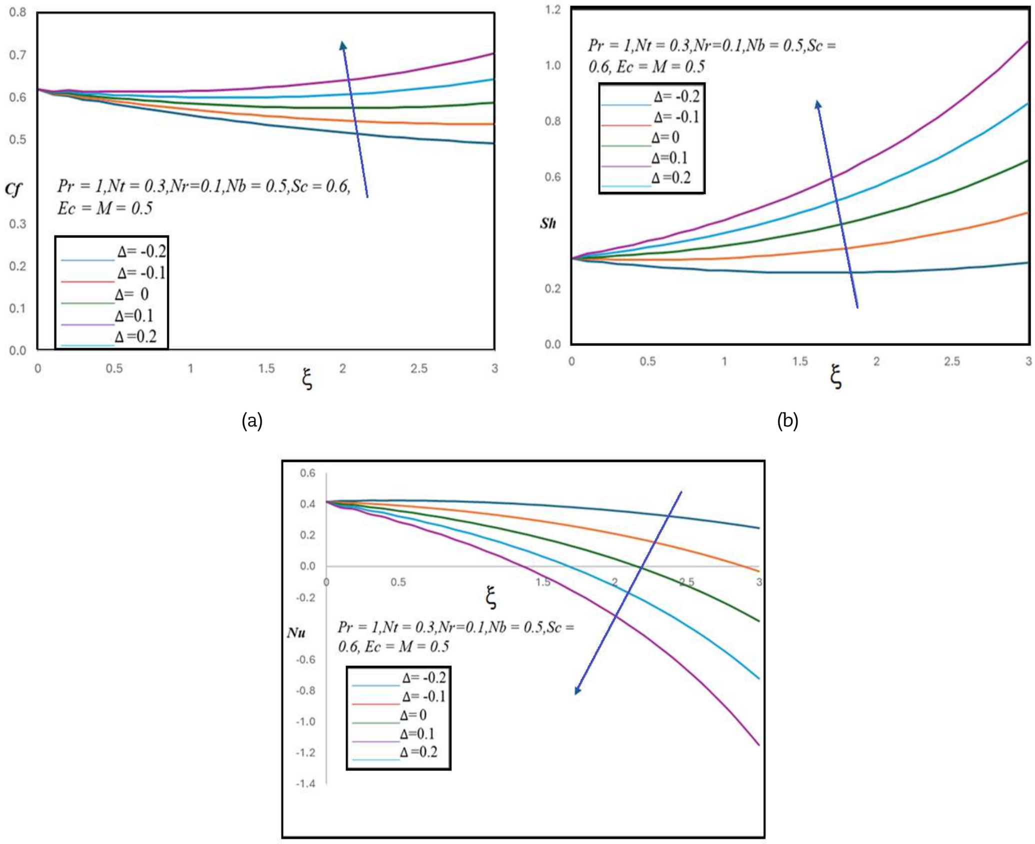

(a) (b)

(c)

Fig. 11. Influence of Δ on (a) skin friction, (b) Sherwood number and, (c) Nusselt number.

Figures 10(a) to 10(c) illuminates the impacts of magnetic factor ($0 \le M \le 2$) on (C_f). (Nu), (Sh) along the surface regime. Magnetic parameter's impact is profound and multifaceted. As magnetic parameter M increases, C_f, (Nu) decreases, while (Sh) increases due to the magnetic field's influence on the Lorentz force. Physically, the Lorentz force opposes the fluid flow, reducing velocity near the surface, which in turn decreases the shear stress, leading to a drop in (C_f). This reduced velocity also weakens convective heat transfer, causing a decline in the (Nu). However, the magnetic field enhances NP diffusion mechanisms such as Brownian motion and thermophoresis, which improve mass transfer, thus increasing the Sh. These effects are characteristic of magnetohydrodynamic (MHD) flows with dissipative and Ohmic heating effects. Thus momentum, and thermal BLT decay, however, concentration BLT is enhanced. These outcomes highlight the importance of understanding magnetic field effects for optimizing heat transfer and reducing energy losses in advanced NF-based technologies across engineering and industrial sectors.

Figures 11(a) to 11(c) Unravels effects of heat generation/absorption ($-0.2 \le \Delta \le 0.2$), on (C_f), (Nu), (Sh) along the surface regime. When heat generation and absorption parameters are appreciated, more thermal energy is added to the fluid, enhancing molecular motion and thus increasing velocity gradients near the surface. This leads to higher skin friction due to intensified fluid-surface interactions. The added thermal energy also promotes NP diffusion, improving mass transfer rates and increasing the Sherwood number. However, the increased internal thermal energy reduces the temperature gradient between fluid and surface, which is essential for effective heat transmission, resulting in a decrease (Nu). Thus, while momentum and mass transmission are enhanced, the efficiency of heat transmission is diminished due to a lower temperature differential. Also, this is applicable in industrial cooling systems, like those in power plants, increased heat generation from machinery raises fluid velocity and enhances mass transfer (like higher skin friction and Sherwood number), but the reduced temperature difference between coolant and equipment results in less efficient heat removal (lower Nusselt number).

Figures 12(a) to 12(c) indicate the implication of (Nb) on, (C_f), (Nu), (Sh) along the surface regime. When the Brownian motion parameter increases, it indicates enhanced random movement of NPs within the fluid. This intensified movement disrupts the fluid layers, increasing velocity gradients near the wall thus raising skin friction. The enhanced NP diffusion due to increased Brownian motion improves mass transfer, resulting in a depreciation in Sh, the graph takes a swirling and twist in a flow. However, this same increased internal particle motion reduces the temperature gradient between fluid and surface by dispersing heat more evenly throughout, resulting to lower Nu. Consequently, while momentum and mass transfer are enhanced, the overall efficiency of heat transfer diminishes due to the more uniform temperature distribution.

Figures 13(a) to 13(c) portray the thermophoresis parameter, (Nt), where ($0 \le Nt \le 0.6$) on (C_f), (Nu), (Sh) along the surface regime. A substantial rise in C_f and Sh as the thermophoresis parameter rises is primarily due to enhanced NP deposition near the surface. Thermophoresis induces NPs to migrate towards regions of a temperature gradient, leading to a higher deposition rate and subsequently increasing C_f, Sh rates. On the contrary, depreciation of Nu occurs because thermophoresis hinders convective heat transfer efficiency. Nanoparticles accumulating near the surface act as thermal barriers, reducing the effective heat transfer area and slowing down convective heat exchange between fluid and surface. Scientifically, these observations are significant in applications involving NFs, such as heat exchangers and thermal coatings. Understanding how thermophoresis affects these parameters helps in maximizing transportation thermal energy processes and creating efficient solutions for thermal control that regulate the deposition of NPs, and the dissipation of heat is critical for performance and operational efficiency.

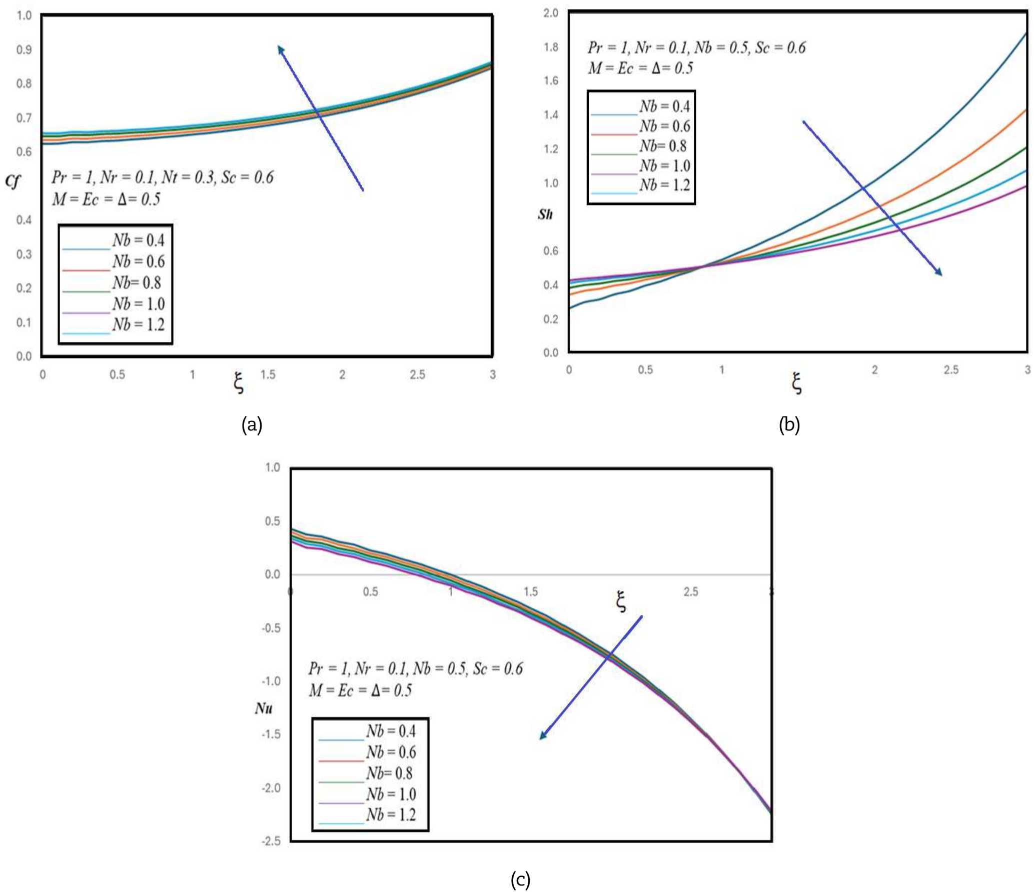

Fig. 12. Influence of *Nb* on (a) skin friction, (b) Sherwood number and, (c) Nusselt number.

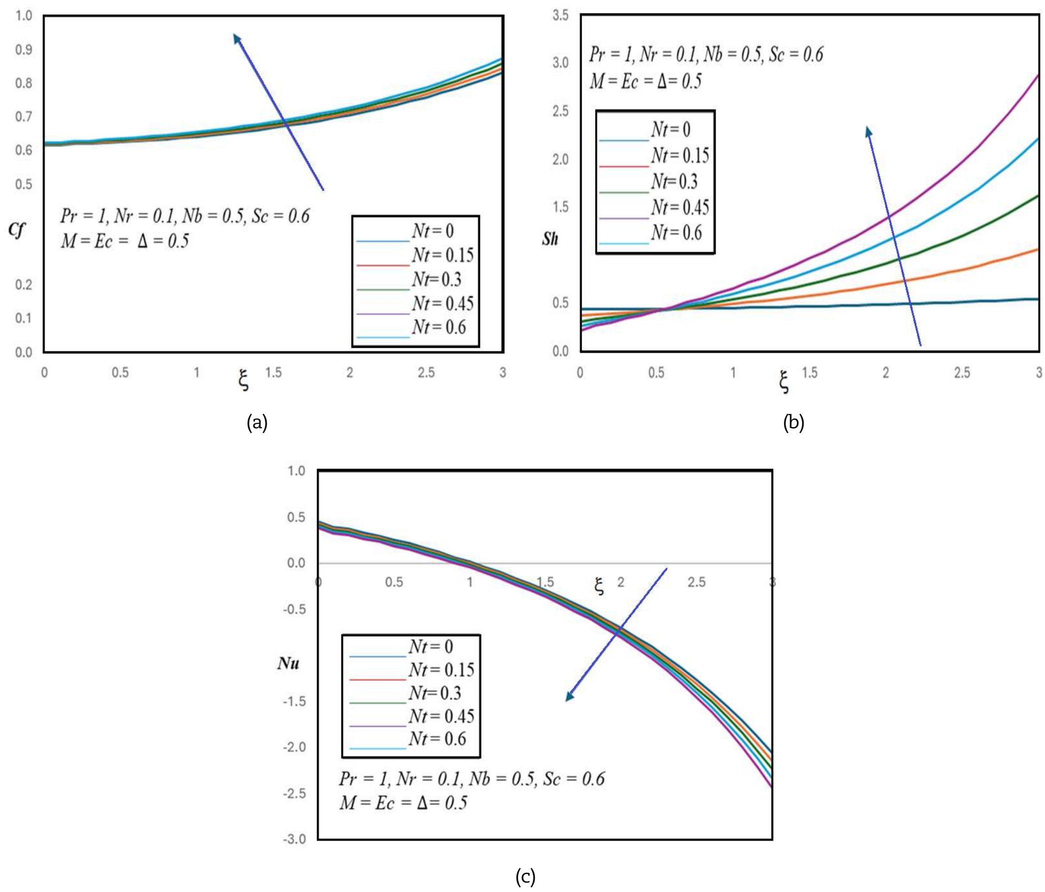

Fig. 13. Influence of *Nt* on (a) skin friction, (b) Sherwood number and, (c) Nusselt number.

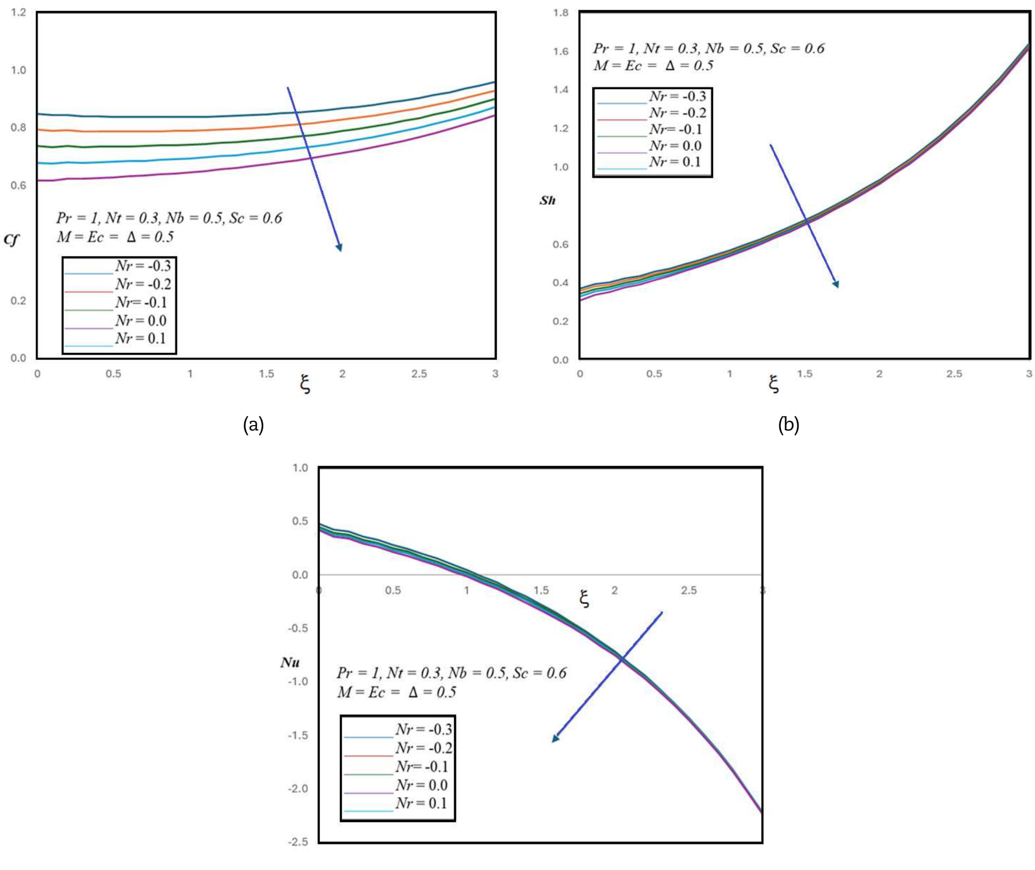

Fig. 14. Influence of *Nr* on (a) skin friction, (b) Sherwood number and, (c) Nusselt number.

Figures 14(a) to 14(c) indicate the buoyancy ratio parameter's impact, (-0.3 ≤ *Nr* ≤ 0.1) on (C_f), (*Nu*), (*Sh*) along the surface regime. When the buoyancy ratio parameter increases, it implies that the effect of buoyancy forces due to concentration gradients becomes more significant relative to those due to thermal gradients. This reduces the overall buoyancy-driven flow, leading to lower velocity gradients near the surface and thus decreasing (C_f) The reduced flow also diminishes mass transfer rates, resulting in a lower Sherwood number. Additionally, the decreased buoyancy effect weakens convective heat transfer, leading to a smaller temperature gradient between fluid, and surface thus reducing *Nu*. Consequently, the overall momentum, mass, and heat transfer rates are diminished due to the decreased implications of thermal (*Nr*) force. In geothermal systems, increasing the buoyancy ratio parameter, such as by injecting solutes, can decrease the effectiveness of thermal-driven convection. This results in lower fluid velocity (reducing skin friction), decreased nutrient or mineral transport (lower Sherwood number), and less efficient heat transport (lower Nusselt number), affecting the overall performance of energy transfer and decaying the momentum, thermal, and concentration BLT.

5. Conclusions

The dissipative magneto-thermal convection flow of Buongiorno's NF through a semi-infinite vertical surface is investigated numerically thermal convection and nanoparticle mass transfer have also been included in the present paper. The conservation equations and boundary conditions have been rendered dimensionless with appropriate scaling non-similarity transformations. The resulting nonlinear multi-physical BVP has then been solved with a second-order implicit finite-difference KBM, implemented in MATLAB 2024b. The Keller box code has been validated with previously published research. Graphical results for the influence of selected parameters on transport characteristics have been presented. Key outcomes of the current analysis are briefly summarized as follows:

a) Substantial converting of kinetic energy into thermal energy via viscous dissipation is indicated by elevated Eckert number *Ec* values, boosting fluid motion, and temperature and reducing local concentration profiles.
b) Higher Magnetic parameter *M* values lead to a reduction in velocity. Conversely, intensified Lorentz forces enhance fluid motion, improving mixing and amplifying thermal and mass transport, resulting in elevated temperature and concentration profiles near the surface.
c) Increased heat generation/absorption Δ elevates fluid temperature, enhancing buoyancy forces and fluid velocity, and a decline in concentration profiles.
d) Increment in Brownian motion *Nb* values leads to enhanced velocity and temperature profiles, while also reducing concentration.
e) Thermophoresis parameter *Nt* increases, nanoparticle deposition near the surface boosts skin friction C_f, Sherwood number *Sh* but reduces Nusselt number *Nu*.
f) Significantly a rise in buoyancy ratio parameter reduces the impact of thermal gradients compared to concentration gradients, leading to decreased fluid velocity, lower skin friction, reduced mass transfer *Sh*, and less efficient heat transfer *Nu*.

The present study has revealed some interesting characteristics of semi-infinite vertical substrate NF boundary layer flows. The combined analysis of the BNFs model and effects of Magnetic parameters, viscous dissipation, Ohmic heating, and heat generation/absorption on non-similar convection flows across a semi-infinite vertical plate constitute the innovations of this work. Keller's box method is very efficient in solving complex multi-physical boundary value problems. However, attention has been confined to the Newtonian case. NFs are known to exhibit rheological effects with a higher volume fraction of nanoparticles. Future investigations may therefore explore non-Newtonian polymeric models including viscoelastic and shear-thinning formulations and additionally, studying NFs response in complex geometries and incorporating detailed boundary conditions, such as time-dependent effects, could better simulate practical scenarios. Leveraging advanced computational techniques, like machine learning and high-performance computing, might further refine simulations and predict nanofluid dynamics under extreme conditions will be communicated soon.

Author Contributions

A. Anjum was responsible for conceptualization, original drafting, editing, and software. S. Abdul Gaffar handled conceptualization, problem formulation and solving, as well as software. S. Kumar contributed to the literature survey and editing. S. Peerusab also contributed to the literature survey and editing. The manuscript was written through the contribution of all authors. All authors discussed the results, and reviewed, and approved the final version of the manuscript.

Acknowledgments

The editor's and reviewers' insightful observations, supportive remarks, and helpful recommendations to enhance the original article are all greatly appreciated by the authors and have helped us in improvising the final draft.

Conflict of Interest

The authors declared no potential conflicts of interest concerning the research, authorship, and publication of this article.

Funding

The authors received no financial support for the research, authorship, and publication of this article.

Data Availability Statements

The datasets generated and/or analyzed during the current study are available from the corresponding author upon reasonable request.

Nomenclature

B	Magnetic field vector (Tesla)
B_0	Constant transverse (radial) magnetic field (Tesla)
P	Pressure (Pa)
D	Nanoparticle diffusivity
C	Nanoparticle volume fraction (-)
T	Temperature of the fluid (Kelvin)
Pr	Prandtl number (-)
Sc	Schmidt number (-)
Gr	Local Grashof number (-)
x	Streamwise coordinate (m)
y	Transverse coordinate (m)
u	Dimensionless velocity components in x direction (m/s)
v	Dimensionless velocity components in y direction (m/s)
Nb	Brownian motion parameter (-)
Nt	Thermophoresis parameter (-)
Nr	Buoyancy ratio parameter (-)
f	Non-dimensional stream function
g	Acceleration due to gravity (m/s^2)
L	Characteristic length (m)
D_B	Brownian diffusion coefficient (m^2/s)
Dm	DMolecular diffusivity (m^2/s)
D_T	Thermophoretic diffusion coefficient (m^2/s)
k	Thermal conductivity of the fluid (W/mK)
k_m	Effective thermal conductivity (W/mK)
T_w	Wall temperature (K)
T_∞	Ambient temperature (K)
C_w	Concentration near Wall (-)
C_∞	Concentration in Ambient stream (-)
V	Velocity vector (m/s)
Nu	Local Nusselt number (surface heat transfer rate) (-)
Sh	Local Sherwood number (surface mass transfer rate) (-)
C_P	Specific heat parameter (J/kgK)
M	Magnetic parameter (-)
C_f	Skin friction coefficient (-)
Greek symbols	
θ	Dimensionless temperature (-)
ϕ	Dimensionless concentration (-)
μ	Dynamic viscosity (kgm/s)
ν	Kinematic viscosity (m^2/s)
ξ	Dimensionless tangential coordinate (-)
η	Dimensionless transverse coordinate (-)
ψ	Dimensionless stream function (-)
μ_f	Dynamic viscosity of base fluid (kg.m^{-1}. s^{-1})
ν_f	Kinematic viscosity of base fluid (m^2/s)
ρ or ρ_f	Density of the base fluid (kg/m^3)
σ or σ_f	Electrical conductivity of the fluid (Siemens/m)
ρ_p	Fluid density of nanoparticles (-)
α or α_m	Thermal diffusivity of the fluid (m^2/s)
β	The thermal expansion coefficient of the fluid (/K)
ρC_p	Effective heat capacity (J/kgK)
τ	The ratio of the effective heat capacity of nanoparticle to the heat capacity of the fluid (-)
Subscripts	
w	Surface conditions
∞	Free stream conditions

References

[1] Choi, S.U.S., Eastman, J.A., Enhancing thermal conductivity of fluids with nanoparticles, *The Proceedings of the ASME International Mechanical Engineering Congress and Exposition, ASME*, San Francisco, USA, 1995, 99-105.
[2] Buongiorno, J., Convective transport in nanofluids, *ASME Journal of Heat and Mass Transfer*, 128, 2006, 240–250.
[3] Kanwal, S., Shah, S.A.A., Bariq, A., Insight into the dynamics of heat and mass transfer in nanofluid flow with linear/nonlinear mixed convection, thermal radiation, and activation energy effects over the rotating disk, *Scientific Reports*, 13, 2023, 23031.
[4] Khan, M.S., Shah, Z., Roman, M., Entropy generation in magneto couple stress nanofluid flow containing gyrotactic microorganisms towards a stagnation point on a stretching/shrinking sheet, *Scientific Reports*, 13, 2023, 21434.
[5] Akbar, A.A., Awan, A.U., Nadeem, S., Ahammad, N.A., Raza, N., Oreijah, M., Guedri, K., Allahyani, S.A., Heat Transfer Analysis of Carreau-Yasuda Nanofluid Flow with Variable Thermal Conductivity and Quadratic Convection, *Journal of Computational Design and Engineering*, 11, 2024, 99–109.
[6] Elboughdiri, N., Dharmaiah, G., Rama Prasad, J.L., Baby Rani, C., Venkatadri, K., Ghernaout, D., Wakif, A., Benguerba, Y., Analysis of a Ferromagnetic Nanofluid Saturating a Porous Medium with Nield's Boundary Conditions, *Mathematics*, 11, 2023, 4579.
[7] Sayyou, H., Belabid, J., Allali, K., Free Convection Nanofluid Flow and Heat Transfer Within a Porous Rectangular Cavity, *Journal of Nanofluids*, 13, 2024, 1030-1039.
[8] Sankar, C.U., Sobhanapuram, S., Devi, S.V.V., Chukka, V., Numerical Study of Natural Convective Flow of a Nanofluid Over Rotating Truncated Cone with Convective Heating, *Journal of Nanofluids*, 13, 2024, 808-818.
[9] Younas, W., Sagheer, M., Enhanced Nanofluid Dynamics and Heat Transfer with Brownian Motion, Chemical Reaction, and Thermophoresis at Stagnation Point, *Journal of Nanofluids*, 13, 2024, 999-1008.
[10] Sheikholeslami, M., Khalili, Z., Scardi, P., Ataollahi, N., Environmental and energy assessment of photovoltaic-thermal system combined with a reflector supported by nanofluid filter and a sustainable thermoelectric generator, *Journal of Cleaner Production*, 438, 2024, 140659.
[11] Usafzai, W.K., Pop, I., Aly, E.H., Steady Gyrostatic Nanofluid Flow past a Permeable Stretching/shrinking Sheet with Velocity Slip Condition using the Nanofluid Model Proposed by Buongiorno, *Journal of Applied and Computational Mechanics*, 10, 2024, 413–421.
[12] Yahyaee, A., Hærvig, J., Sørensen, H., Nanoparticle migration in nanofluid film boiling: A numerical analysis using the continuous-species-transfer method, *International Journal of Heat and Mass Transfer*, 224, 2024, 125344.
[13] Chen, J., Liang, C., Lee, J.D., Micropolar electromagnetic fluids: control of vortex shedding using imposed transverse magnetic field, *J. Advanced Mathematics and Applications*, 1, 2012, 151–162.
[14] Renu, K., Kumar, A., Effect of Wall Conductivity on Mixed Convection Magnetohydrodynamic Nanofluid Flow with Thermal Non-Equilibrium Approach in Vertical Channel, *Journal of Nanofluids*, 13, 2024, 873–888.
[15] Tang, T.Q., Shah, Z., Thumma, T., Response surface optimization and sensitive analysis on biomagnetic blood Carreau nanofluid flow in stenotic artery with motile gyrotactic microorganisms, *SN Applied Sciences*, 5, 2023, 355.
[16] Islam, T., Alam, M.N., Niazai, Heat generation/absorption effect on natural convective heat transfer in a wavy triangular cavity filled with nanofluid, *Scientific Reports*, 13, 2023, 21171.
[17] Rehman, K.U., Shatanawi, W., Al-Mdallal, Q.M., A comparative remark on heat transfer in thermally stratified MHD Jeffrey fluid flow with thermal radiations subject to cylindrical/plane surfaces, *Case Studies in Thermal Engineering*, 32, 2022, 101913.
[18] Razzaq, R., Farooq, U., Cui, J., Muhammad, T., Non-similar solution for the magnetized flow of Maxwell nanofluid over an exponentially stretching surface, *Mathematical Problems in Engineering*, 2021, 5539542.
[19] Ashraf, M.U., Qasim, M., Wakif, A., Afridi, M.I., Animasaun, I.L., A generalized differential quadrature algorithm for simulating the magnetohydrodynamic peristaltic flow of blood-based nanofluid containing magnetite nanoparticles: a physiological study, *Numerical Methods for Partial Differential Equations*, 38, 2022, 666–692.
[20] Ahmad, S., Hayat, T., Alsaedi, A., Ullah, H., Shah, F., Computational modeling and analysis for the effect of magnetic field on rotating stretched disk flow with heat transfer, *Propulsion and Power Research*, 10, 2021, 48–57.
[21] Jan, A., Mushtaq, M., Farooq, U., Hussain, M., Non-similar analysis of magnetized Siskonanofluid flow subjected to heat generation/absorption and viscous dissipation, *Journal of Magnetism and Magnetic Materials*, 564(2), 2022, 170153.
[22] Hussain, M., Cui, J., Farooq, U., Rabie, M. E. A., Muhammad, T., Non-similar modeling and numerical simulations of the electromagnetic radiative flow of nanofluid with entropy generation, *Mathematical Problems in Engineering*, 20, 2022, 4272566.
[23] Gangadhar, K., Kumari, M. A., Chamkha, A. J., EMHD flow of radiative second-grade nanofluid over a Riga Plate due to convective heating: Revised Buongiorno's nanofluid model, *Arabian Journal for Science and Engineering*, 47(7), 2022, 8093-8103.
[24] Reddy, R., Gaffar, S. A., Chemical Reaction and Viscous Dissipative Effects on Buongiorno's Nanofluid Model Past an Inclined Plane: A Numerical Investigation, *International Journal of Applied and Computational Mathematics*, 10(2), 2024, 1-20.
[25] Santhosh, N., Sivaraj, R., Prasad, V. R., Beg, O. A., Leung, H. H., Kamalov, R., Kuharat, S., Computational study of MDD mixed convective flow of Cu/Al2O3-water nanofluid in a porous rectangular cavity with slits, viscous heating, Joule dissipation, and heat source/sink effects, *Waves in Random and Complex Media*, 2023, 1-34. https://doi.org/10.1080/17455030.2023.2168786
[26] Pal, D., Das, B. C., Vajravelu, K., Magneto-Soret-Dufour thermo-radiative double-diffusive convection heat and mass transfer of a micropolar fluid in a porous medium with Ohmic dissipation and variable thermal conductivity, *Propulsion, and Power Research*, 11(1), 2022, 154-170.
[27] Sharma, B. K., Gandhi, R., Combined effects of Joule heating and non-uniform heat source/sink on unsteady MHD mixed convective flow over a vertical stretching surface embedded in a Darcy-Forchheimer porous medium, *Propulsion, and Power Research*, 11(2), 2022, 276-292.
[28] Li, S., Khan, M. I., Alzahrani, F., Eldin, S. M., Heat and mass transport analysis in radiative time-dependent flow in the presence of Ohmic heating and chemical reaction, viscous dissipation: An entropy modeling, *Case Studies in Thermal Engineering*, 42, 2023, 102722.
[29] Khan, W. U., Awais, M., Parveen, N., Ali, A., Awan, S. E., Malik, M. Y., He, Y., Analytical Assessment of (Al2O3–Ag/H2O) Hybrid Nanofluid Influenced by Induced Magnetic Field for Second Law Analysis with Mixed Convection, Viscous Dissipation, and Heat Generation, *Coatings*, 11, 2021, 498.
[30] Shahzad, F., Jamshed, W., Nisar, K. S., Khashan, M. M., Abdel-Aty, A. H., Computational analysis of Ohmic and viscous dissipation effects on MHD heat transfer flow of Cu-PVA Jeffrey nanofluid through a stretchable surface, *Case Studies in Thermal Engineering*, 26, 2021, 101148.
[31] Hayat, T., Khan, S. A., Alsaedi, A., Irreversibility characterization in nonliquid flow with velocity slip and dissipation by a stretchable cylinder, *Alexandria Engineering Journal*, 60, 2021, 2835-2844.
[32] Sarkar, B., Laminar forced convection MHD Couette-Poiseuille flow with viscous and Joule dissipations, *Journal of Scientific Research*, 14(3), 2022, 877–889.
[33] Shamshuddin, M., Narayana, P. S., Combined effect of viscous dissipation and joule heating on MHD flow past a Riga plate with Cattaneo–Christov heat flux, *Indian Journal of Physics*, 94(9), 2020, 1385–1394.
[34] Mng'ang'a, J., Effects of Ohmic heating, induced magnetic field and Newtonian heating on magnetohydrodynamic generalized Couette flow of Jeffrey nanofluid between two parallel horizontal plates with convective cooling, *International Journal of Thermofluids*, 20, 2023, 100402.
[35] Saleel, A. C., Alshahrani, S. A., Afzal, A., Baig, M. A. A., Kamangar, S., Khan, T. M., Flow control in microfluidics devices: Electro-osmotic Couette flow with joule heating effect, *Frontiers in Engineering and Built Environment*, 1(2), 2021, 146-160.
[36] Shamshuddin, M., Mishra, S., Bég, O. A., Kadir, A., Viscous dissipation and joule heating effects in non-Fourier MHD squeezing flow, heat and mass transfer between Riga plates with thermal radiation: Variational parameter method solutions, *Arabian Journal for Science and Engineering*, 44(9), 2019, 8053–8066.
[37] Ramesh, K., Effects of viscous dissipation and Joule heating on the Couette and Poiseuille flows of a Jeffrey fluid with slip boundary conditions, *Propulsion and Power Research*, 7(4), 2018, 329–341.

[38] Mansour, A. M., Chamkha, A. J., Mohamed, R. A., El-Aziz, M. M. A., Ahmed, S. E., MHD natural convection in an inclined cavity filled with a fluid-saturated porous medium with a heat source in the solid phase, *Nonlinear Analysis: Modelling and Control*, 15, 2010, 82.
[39] Mahapatra, T. R., Pal, D., Mondal, S., Mixed convection in a lid-driven square cavity filled with porous medium in the presence of thermal radiation and non-uniform heating, *International Communications in Heat and Mass Transfer*, 41, 2013, 55.
[40] Umadevi, P., Nithyadevi, N., Magneto-convection of water-based nanofluids inside an enclosure having uniform heat generation and various thermal boundaries, *Journal of the Nigerian Mathematical Society*, 35, 2016, 82.
[41] Alagumalai, A., Qin, C., KE K, V., Solomin, E., Yang, L., Zhang, P., Otanicar, T., Kasaeian, A., Chamkha, A. J., Rashidi, M. M., Wong Wises, S., Ahn, H. S., Lei, Z., Saboori, T., Mahian, O., Conceptual analysis framework development to understand barriers of nanofluid commercialization, *Nano Energy*, 92, 2022, 106736.
[42] Tayebi, T., Dogonchi, A. S., Karimi, N., Ge-JiLe, H., Chamkha, A. J., Elmasry, Y., Thermo-economic and entropy generation analyses of magnetic natural convective flow in a nanofluid-filled annular enclosure fitted with fins, *Sustainable Energy Technologies and Assessments*, 46, 2021, 101274.
[43] Chamkha, A. J., Dogonchi, A. S., Ganji, D. D., Magnetohydrodynamic nanofluid natural convection in a cavity under thermal radiation and shape factor of nanoparticles impacts: A numerical study using CVFEM, *Applied Sciences*, 8, 2018, 2396.
[44] Pohlhausen, E., Der Wärmeaustausch zwischen festen Körpern und Flüssigkeiten mit kleiner Reibung und kleiner Wärmeleitung, *ZAMM-Journal of Applied Mathematics and Mechanics/Zeitschrift für Angewandte Mathematik und Mechanik*, 1(2), 1921, 115-121.
[45] Ostrach, S., An analysis of laminar free-convection flow and heat transfer about a flat plate parallel to the direction of the generating body force, *NACA-TR-1111*, 1953.
[46] Gebhart, B., Pera, L., The nature of vertical natural convection flows resulting from the combined buoyancy effects of thermal and mass diffusion, *International Journal of Heat and Mass Transfer*, 14, 1971, 2025–2050.
[47] Gebhart, B., Jaluria, Y., Mahajan, R. L., Sammakia, B., *Buoyancy induced flows and transport*, Hemisphere, Washington, DC, 1988.
[48] Awati, V. B., Kumar, N. M., Analysis of forced convection boundary layer flow and heat transfer past a semi-infinite static and moving flat plate using nanofluids-by Haar wavelets, *Journal of Nanofluids*, 10(1), 2021, 106-117.
[49] Yao, C., Li, B., Si, X., Meng, Y., On fluid flow and heat transfer of turbulent boundary layer of pseudoplastic fluids on a semi-infinite plate, *Physics of Fluids*, 32(7), 2020.
[50] El-Dabe, N. T., Gabr, M. E., Elshekhipy, A. A., Zaher, S. A., The motion of a non-Newtonian nanofluid over a semi-infinite moving vertical plate through porous medium with heat and mass transfer, *Thermal Science*, 24(2 Part B), 2020, 1311-1321.
[51] Choudhury, K., Sharma, S., MHD free convective heat and mass transfer flow passing through the semi-infinite plate for Cu-water and TiO2-water nanofluids in presence of radiation embedded in a porous medium, *ZAMM-Journal of Applied Mathematics and Mechanics/Zeitschrift für Angewandte Mathematik und Mechanik*, 104, 2024, e202300851.
[52] Keller, H. B., Numerical Methods in Boundary-Layer Theory, *Annual Review of Fluid Mechanics*, 10, 1978, 417-433.
[53] Gaffar, S. A., Bég, O. A., Prasad, V. R., Khan, B. M. H., Kadir, A., Computation of Eyring-Powell micropolar convective boundary layer flow from an inverted non-isothermal cone: thermal polymer coating simulation, *Computational Thermal Sciences*, 12(4), 2020, 329–344.
[54] Gaffar, S. A., Bég, O. A., Kuharat, S., Bég, T. A., Computation of hydromagnetic tangent hyperbolic non-Newtonian flow from a rotating non-isothermal cone to a non-Darcy porous medium with thermal radiative flux, *Physics Open*, 19, 2024, 100216.
[55] Bég, O. A., *Numerical Methods for Multi-Physical Magnetohydrodynamics, New Developments in Hydrodynamics Research*, Ibragimov, M. J., Anisimov, M. A. (Eds.), Nova Science, New York, 1–110, Chap. 1, 2012.
[56] Reddy, P. R., Gaffar, S. A., Bég, O. A., Khan, B. M. H., Hall and ion-slip effects on nanofluid transport from a vertical surface: Buongiorno's model, *ZAMM-Journal of Applied Mathematics and Mechanics/Zeitschrift für Angewandte Mathematik und Mechanik*, 102(3), 2022, e202000174.
[57] Abbas, T., Khan, S. U., Saeed, M., Khan, M. I., Ismail, E. A. A., Awwad, F. A., Abdullaeva, B. S., Thermal stability and slip effects in micropolar nanofluid flow over a shrinking surface: A numerical study via Keller box scheme with block-elimination method, *AIP Advances*, 14(8), 2024.
[58] Chen, T. S., Tien, H. C., Armaly, B. F., Natural convection on horizontal, inclined, and vertical plates with variable surface temperature or heat flux, *International Journal of Heat and Mass Transfer*, 29(10), 1986, 1465-1478.
[59] Narahari, M., Unsteady free convection flows past a semi-infinite vertical plate with constant heat flux in water-based nanofluids, *IOP Conference Series: Materials Science and Engineering*, 342(1), 2018, 012085.
[60] Ramya, D., Raju, R. S., Rao, J. A., Chamkha, A. J., Effects of velocity and thermal wall slip on magnetohydrodynamics (MHD) boundary layer viscous flow and heat transfer of a nanofluid over a non-linearly stretching sheet: a numerical study, *Propulsion and Power Research*, 7(2), 2018, 182-195.
[61] Prasad, V. R., Gaffar, S. A., Reddy, E. K., Bég, O. A., Flow and heat transfer of Jefferys non-Newtonian fluid from a horizontal circular cylinder, *Journal of Thermophysics and Heat Transfer*, 28(4), 2014, 764-770.
[62] Gaffar, S. A., Prasad, V. R., Reddy, E. K., Computational study of Jeffrey's non-Newtonian fluid past a semi-infinite vertical plate with thermal radiation and heat generation/absorption, *Ain Shams Engineering Journal*, 8(2), 2017, 277-294.

ORCID ID

Asra Anjum https://orcid.org/0009-0002-7878-6798
Shaik Abdul Gaffar https://orcid.org/0000-0002-7368-1658
Sateesh Kumar https://orcid.org/0000-0001-8141-2899
Samdani Peerusab https://orcid.org/0000-0003-0434-2772

How to cite this article: Anjum A., Gaffar S.A., Kumar S., Peerusab S. Dissipative Magneto-thermo-convection of Nanofluid Past through a Semi-infinite Vertical Surface with Ohmic Heating, *J. Appl. Comput. Mech.*, 11(4), 2025, 991-1008. https://doi.org/10.22055/jacm.2024.47689.4765